3D morphology and timing of the giant fossil pockmark of Beauvoisin, SE Basin of France

Aurélien Gay, Michel Lopez, Jean-Luc Potdevin, Valérie Vidal, German Varas, Alexiane Favier, Nicolas Tribovillard

3D morphology and timing of the giant fossil pockmark of Beauvoisin, SE Basin of France

Aurélien Gay[1], Michel Lopez[1], Jean-Luc Potdevin[2], Valérie Vidal[3], German Varas[4], Alexiane Favier[1,5], Nicolas Tribovillard[2]

1 Géosciences Montpellier, UMR CNRS 5243, Université de Montpellier, F-34095 Montpellier, France

2 Laboratoire d'Océanologie & Géosciences, UMR CNRS 8187, Université de Lille 1, F-59655 Villeneuve d'Ascq, France

3 Laboratoire de Physique, ENS de Lyon, CNRS, Université de Lyon, F-69342 Lyon, France

4 Instituto de Física, Pontificia Universidad Católica de Valparaíso, Av. Universidad 330, Valparaíso, Chile

5 Géoazur Nice, UMR CNRS 7329, Université de Nice-Sophia Antipolis, F-06560 Valbonne, France

* Corresponding author: Aurélien Gay, Géosciences Montpellier, Université de Montpellier, Case 060, Place Eugène Bataillon, 34095 Montpellier Cedex 5, FRANCE. Tel: +33 (0) 4 67144598, E-mail address: aurelien.gay@umontpellier.fr

Number of words of text: (without abstract, bibliography and figure caption): 8584

Number of references: 91

Number of figures: 13

Abbreviated title: Morphology and timing of a fossil giant pockmark

1. Abstract

The resolution of data acquired over modern seafloors does not allow imaging of the inner features of a fluid seep structure, particularly in the shallow subsurface. In the South-East Basin of France (Drôme), fossil cold seep structures comprising fossil-rich carbonate lenses were identified about 30 years ago within the Oxfordian (Late Jurassic) Terres Noires Formation. These structures were first interpreted as pseudo-bioherms related to hydrothermal activity, but comparison with active seep sites on modern margins, together with isotopic analyses led to a re-interpretation involving cold fluids instead. To date, all seep sites have generally been studied individually without considering any link to neighboring or more distant sites. Based on 23 high-resolution stratigraphic logs within the structure coupled to mosaicked aerial photographs from a drone survey, the 19 fluid seep events were correlated in the area, including two new sites exposed due to weathering. We have shown that each identified sub-site is composed of sub-vertically

stacked fossil-rich carbonate lenses interbedded with marls, which developed in smooth, 4 to 6 m deep depressions beneath the local seabed. The nodules present within the depressions are of primary importance as they mark the area of active seeping. This general organization is very similar to the modern Regab giant pockmark in the Lower Congo Basin where only a few sub-sites are active at the same time. A spatio-temporal 3D reconstruction of the position of these sub-sites shows that the carbonate lenses are organized into clusters comprising up to 7 sub-sites grouped together in the same stratigraphic interval and the same geographic zone. A sandbox experiment where gas is injected at constant flow rate at the base of a box filled with a matrix of water-saturated grains displays a pattern consisting of disturbed sediments inside a parabolic-shaped area. This parabolic shape was also identified on a seismic profile across the Regab giant pockmark, suggesting that the processes are similar for the Beauvoisin and Regab seep areas. The laboratory experiments also show that the seeping conduit is stable during a given period of time and suddenly shifts laterally. It is mainly due to the collapse of the conduit, the lateral migration and the reopening at a new position. The general log obtained in the Beauvoisin seep area suggests a similar pattern with periods of seeping alternating with periods of quiescence, each of which is approximately 200 ka. Even if a pockmark seems to have been inactive for a long period of time, it could be due to the lateral shift of the feeder conduit meaning that the sub-seafloor is still charged in gas. This is of primary importance for risk assessment, hydrocarbon exploration and general understanding of geobiology at seafloor seeps.

200 words short abstract:

In the SE Basin of France (Drôme), fossil cold seep structures made of fossil-rich carbonate lenses were identified in the Oxfordian (Late Jurassic) Terres Noires Formation about 30 years ago. To date, all seep sites have generally been studied individually without consideration of any link to neighboring or more distant sites. Based on a detailed fieldwork in the Beauvoisin area and comparison with the modern, active giant Regab pockmark and sandbox experiments, we suggest that this site can now be considered as a 800 m wide fossil analogue of a giant pockmark. It comprises several 4-6 m deep, 80-120 m wide coalesced sub-seep sites. A spatio-temporal 3D reconstruction of the position of these sub-sites shows that the carbonate lenses are organized in clusters with only one cluster active at a given period. Two periods of seep activity are separated by a period of quiescence due to the lateral shift of the feeder conduit beneath the structure. This suggests that even if a seafloor pockmark appears to be inactive, this could be due to the lateral shift of the feeder conduit meaning that the sub-seafloor is still charged in gas.

2. Introduction

Hydrogen sulfide and methane that sustain highly specialized chemosynthetic-based ecosystems in cold seep environments have been recognized in many modern basins worldwide (***Campbell, 2006; Amano et al., 2010; Teichert and Van de Schrootbrugge, 2013***) and in the fossil record in the early Cenozoic - onwards (***Campbell et al., 1995b; Kiel and Little, 2006; Kiel, 2010; Vrijenhoek, 2013***). Sulfide and methane

release results in carbonate precipitation forming lenses encased in surrounding limestones or marlstones (*Campbell et al., 2002*). These fossil organism-rich, authigenic, carbonate rocks developed at the seafloor where oil and/or gas migrated from an underlying network of focused fluid flow in sedimentary basins (*Bohrmann et al., 1998; Aloisi et al., 2000; Aloisi et al., 2002*). The fossils dominated by lucinid bivalves generally show larger dimensions than at other sites as they rely on chemotrophic symbionts for nutrition (*Paull et al., 1992*). This biogeochemical process mainly relies on anaerobic oxidation of methane (AOM) (*Boetius et al., 2000*), where the symbiotic consortia of sulfate-reducing bacteria and methanotrophic archaea use both sulfate and methane for their metabolism and biomass synthesis, thus supplying energy and nutriments to their hosts (*Knittel and Boetius, 2009; Deusner et al., 2014*). However, fossil-rich carbonate assemblages have always been considered as individual seep sites without comparing their distribution to the geometrical organization of modern clusters of seep sites. This lack of connection between isolated seep sites can be due 1) to poor outcrop conditions or stratigraphic uncertainty (*Natalicchio et al., 2015*), or 2) to the large size of modern pockmarks that are several hundred meters in diameter and a few meters only in depth (typically 500-800 m wide and 5-80 m deep) leading to difficult or incorrect correlations in the field (*Gay, 2002; Stewart, 2015*). To date, a fossil giant pockmark has never been identified nor characterized at outcrop, although some microbial assemblages have been reinterpreted in the light of examination of modern hot vents at mid-ocean ridges and cold seeps at continental margins (*Whiticar, 1999; Gay et al., 2006*). This is the case for the fossil seep sites in the Jurassic limestones of Beauvoisin in the SE Basin of France, which were first interpreted as hydrothermal vents (*Rolin, 1987*; Gaillard et al., 1996**)** and then reinterpreted as cold seeps (*Peckmann et al., 1999; Kiel, 2013*). The Beauvoisin seep site is of high importance as it is one of the few worldwide examples that is equivalent to Cenozoic chemosymbiotic-related fossil sites (*Campbell et al., 1995a; Louis-Schmid et al., 2007*). All seep sites have been generally studied individually without consideration of any link to neighboring sites even those situated in more distant locations (*Louis-Schmid et al., 2007*). Furthermore, in the fossil record isolated carbonate lenses or -groups of small-scale carbonate lenses, about 10 m wide and 5 m high, have often been considered as individual pockmarks or as a field of pockmarks respectively (*Agirrezabala et al., 2013*).

The aim of this paper is to characterize the 3D architecture of a 800 m-wide cluster of fossil seep sites at Beauvoisin in the SE Basin of France, in the vicinity of Buis les Baronnies and Propiac (Drôme) (**Fig. 1**), based on the correlation of detailed sedimentological logs, sampling of key seep features such as carbonate lenses, marls, nodules and related petrographical and geochemical analyzes. The Beauvoisin architecture is then compared to that of the Regab giant pockmark in the Lower Congo Basin and to sandbox and numerical models simulating fluid injection at the base of a box filled with a matrix of water-saturated grains.

3. Methods and data

Since the first studies of the Beauvoisin site conducted in the 80's (***Gaillard et al., 1985***; ***Rolin, 1987, Rolin et al., 1990***), recent erosion has exposed new sites and to date, 19 embedded carbonate masses (sub-sites A to T, **see Fig. 2 for location**) have been identified at various positions in the stratigraphic record, using the initial nomenclature of ***Rolin*** (***1987***). This suggests that all sites are not cropping out due to vegetal cover and agricultural fields and some sub-sites are probably still to be found. In order to define precisely the stratigraphical relationship between the encasing fine-grained marls and the fossil-rich carbonate units, twenty-three stratigraphical logs were obtained through the entire area using a Jacob's stick, between 2002 and 2016. The precision is about 2 cm for each log. Field analysis of the Beauvoisin unit comprises identification of major stratigraphic and sedimentological features. The general correlation is related to the Tethyan sequences (***Gradstein et al., 2012***) and some key layers were easily identified (**Fig. 3**), such as the few cm-thick bentonite layers documented by ***Pellenard,*** **(*2003***), or the sub-continuous 10 cm to 1 m thick layers of massive carbonate layers R1 to R20 of the Argovian sequence identified by ***Gaillard et al.*** (***1992***). This study is then based on the analysis of the macroscopic fabric of carbonate lenses related to the reference layers in the surrounding marls of the "Terres Noires" Formation. Sampling for petrographical, mineralogical and geochemical analyses of the carbonate deposits was carried out on steep slopes in marls. Where thalwegs were not accessible for sampling or mapping, a drone was used for high-resolution photography. The obtained mosaics were coupled to aerial photographs and then georeferenced to topographic maps (IGN map #3140ET) in order to establish the areal distribution of outcrop (**Fig. 2**).

Analyses were conducted at the University of Barcelona for C and O isotopes. Forty-eight microsamples were prepared after the petrographic study to determine the carbon and oxygen stable isotope ratio of the different cements using the standard technique of Craig and Gordon (1965) and Claypool et al., (1980). The CO_2 was extracted from 60±10 µg of powdered carbonate samples which were reacted with 103% phosphoric acid for 2 min at 70° C for calcites. The CO_2 was analyzed using an automated Kiel Carbonate Device attached to a Thermal Ionization Mass Spectrometer Thermo Electron (Finnigan) MAT-252. The results are precise to ±0.02‰ for $\delta^{13}C$ and ±0.04‰ for $\delta^{18}O$.

The general organization of the fossil seep sites of Beauvoisin was then compared to the modern and active Regab pockmark in the Lower Congo Basin (***Ondreas et al., 2005; Gay, 2002; Gay et al., 2006; Marcon et al., 2014***). Bathymetry and imaging data were acquired during various surveys between 1999 (ZAIANGO) and 2011 (WACS) using IFREMER's remotely operated vehicle (ROV) *Victor 6000*. The first survey was conducted during a site exploration and mosaicking at about 2 m above the sea-bottom. The main survey was then conducted from 30 m above the seafloor using a Reson Seabat 7125 multibeam echosounder (MBES) running at 400 kHz.

The sandbox model consists of a Plexiglas cylindrical tank (24 cm diameter) for the 3D and a vertical Hele-Shaw cell (glass plates 40 × 30 cm, separated by a 2 mm gap) for the 2D laboratory experiments. Both

systems are filled with particles immersed in water and a constant flow of air, Φ, is injected from a single inlet centered at the base of the cell. The particles are polydispersed, spherical glass beads (Sovitech glass spheres), sieved to obtain four batches with particle diameters d = 218 ± 17, 318 ± 44, 631 ± 37, and 802 ± 68 μm. The grain size distribution for the different batches is measured by means of a microscope (Optika B-163) and roughly displays a Gaussian shape (***Ramos et al., 2015***). In the 2D experiment the grain dynamics are tracked by analyzing the absolute difference in the intensity of two consecutive images, which gives access to regions where motion occurred in the immersed granular layer, due to the ascending gas flow. In order to quantify the generation of the fluidized zone, which corresponds to a cumulative process due to the continuous gas emission, we define the normalized flow density, computed as the cumulation of successive image differences (***Ramos et al., 2015; Varas et al., 2015; Poryles et al., 2016***). This variable makes it possible to quantify the regions where motion occurred (disturbed particles).

4. Geological setting

The Beauvoisin seep site is located in the northern part of the South East Basin of France (**Fig. 1**) which is related to the Jurassic opening of the Liguro-tethyian Ocean (***Lemoine 1985***). From the Hettangian to the Bathonian the basin was a shallow-water carbonate platform with frequent subaerial exposure or erosion indicating a stable margin with a low rate of subsidence. From the Bathonian, sedimentation compensated for the moderate subsidence of the southern platform and environments remained shallow, whereas along the northern platform cherts and organic-rich marls indicate a general deepening of at least 600 m (***Dardeau, 1988***). From the Oxfordian, general subsidence affected the entire platform, moderate in the southern part (reefal facies and confined environments) and increasing in the northern part (deep marl facies and submarine slides).

In the Beauvoisin area the identified seep sites occur in the deepest, central part of the basin where the subsidence was at a maximum from the Bathonian to the Oxfordian (***Gaillard et al. 1985***). This led to deposition of up to 2000-2500 m of organic-rich marls called the "Terres Noires" Formation, limited to the North by the Jura high, to the West by the Cevennes domain and to the East by the Briançonnais domain of the Western Alps (**Fig. 1**). The "Terres Noires" Formation has also been identified in boreholes in the south in Camargue and Provence (***Dardeau, 1988***). Subsidence was mostly due to basement faults with kinematics controlled by salt withdrawal in the extensional domain of the margin (***Mascle et al, 1988***). The fluid seep sites are bounded to the west by major salt-rooted faults which facilitated growth of the main salt diapirs into the marls, as at Propiac and Condorcet (**Fig. 1**).

The "Terres Noires" Formation is divided into three main intervals corresponding to the three major geodynamical episodes that affected the margin ***(Gaillard et al., 1985; Gaillard et al., 1988; Rolin, 1987; Rolin et al., 1990)***. The Bathonian sequence is characterized by marls alternating with thin mudstone layers. The Callovian to Middle Oxfordian sequence is dominated in the lower part by cm to pluri-cm thick dolomudstones and in the middle and upper part by marls containing isolated red to grey nodules

("Nodules Chocolat" by ***Artru, 1972***). The upper Oxfordian is composed of marls alternating with pluri-cm to m thick dolomudstones layers in a general thickening upward sequence. The transition to the Kimmeridgian is marked by the Argovian sequence composed of thick amber dolomudstone layers alternating with light brown marls.

To date the origin of focused fluids has never been clearly elucidated. They were hypothetically related to crustal faults (***Lemoine, 1988***), to halokinesis (***Mascle et al, 1988***) or to biogenic origin derived from the decomposition of organic matter contained in the "Terres Noires" Formation (***Gaillard et al., 1996***). Fluorescence conducted on fluid inclusions coupled to stable carbon isotope analyses have shown the presence of oil containing n-alkanes generated from thermal maturation of organic matter from the sedimentary pile (***Peckman et al., 1999***). The latter is consistent with the total thickness of the "Terres Noires" Formation which has clearly reached a burial depth through the oil window in the lower part.

5. Log correlations

The fossil-rich carbonate suite of Beauvoisin crops out within the thick succession of well-stratified Jurassic marls of the "Terres Noires" Formation in the Lower to Upper Oxfordian interval (***Gaillard et al. 1985***). Between 2002 and 2016, 23 stratigraphical logs were collected allowing a detailed correlation of the 19 sites (A to T) related to the general stratigraphy of the Oxfordian marls (**Fig. 2**). All sites are concentrated west of Beauvoisin and south of the "Col de la Taillade" (**Fig. 2**) where they are exposed in very steep valleys between 660 m and 870 m altitude. This work is based on the initial nomenclature established by ***Gaillard et al. (1985) and Rolin (1987)***. They grouped together carbonate lenses in sites from A to R (***Rolin et al., 1990***). The intense weathering in spring and fall in the region for the last 30 years allowed 2 new sites to be exposed in the Terres Noires Formation. The sites S and T were integrated into the general stratigraphy of Beauvoisin in Logs 11 and 15, respectively (**Fig. 2**).

The 23 stratigraphical logs were constrained using key layers, R1 to R20 following the nomenclature of ***Gaillard et al. (1985) and Rolin (1987)***. However, additional layers (not displayed in this study) were also used following ***Gaidon (1988), Pellenard et al. (1999) and Pellenard et al. (2003)***. This included the identification of a bentonite layer, located at about 220 m above the bottom of Log 1 (**Fig. 3**), which is the reference for all measurements in this study. Some cm-thick ochre and gypsum-rich layers were also recognized in the area. They can be correlated over all the basin and mark some regional events ***(Pellenard et al., 1999)***. The correlation is centered and flattened on the R1 level corresponding to the base of the Argovian sequence ending on top with the R6 level. It is characteristic of the upper part of the Oxfordian in the SE Basin of France and it is composed of dm to m, yellowish to light brown, limestones alternating with light grey marls and claystones.

It is worth noting that the thicknesses of the Argovian sequence varies by a factor of 3 to 4 over a distance of 700 m which is the longest distance between two logs in the area. For instance, this is the case for the

R2-R6 interval which is about 110 m thick in log 16 (North), 60 m thick in log 8 (centre of the area), 30 m thick in log 9 (West) and 90 m thick in log 13 (South West) (**see Fig. 2 for location**). In particular, log 9 shows evidence of intense deformations due to slumps at 260 m and 275 m (**Fig. 3**). The thickness variations in the Argovian sequence could be due to syn-to-post depositional erosion or slump processes which increase towards the centre of the area.

Based on the log correlation it is then possible to generate a composite log taking into account the eroded missing sequences, slump deposits and faults (**Fig. 4**). When varying laterally, the thickest part of a sequence was kept in order to correspond to the 360 m total thickness of the studied Oxfordian interval. On this composite log, the oldest site A is located within the Cordatum Zone (Lower Oxfordian) whereas the youngest site T is in the Bifurcatis Zone (Upper Oxfordian). Given the uncertainty of absolute dating in the Jurassic, the Tethysian sequences and age model from ***Gradstein et al. (2012)*** are reported on the right side as an indication only. It shows that only two sites (A and S) developed in the *Cordatum Zone* corresponding to the Lower Oxfordian whereas most sites developed in the *Plicatilis Zone* (B, C, D, E, F, G, H, I, J, K) and in the Transversarium Zone (L, M, N, O, P, Q, R, T) that are Middle Oxfordian in age and only 2 sites (R and T) developed in the *Bifurcatis Zone* corresponding to the Upper Oxfordian (**Fig. 4**). Given an average rate of sedimentation and a constant compaction rate within the interval, 310 m were deposited in 3.1 Ma between 157,4 and 160,5 Ma. The base of site A1 at 15 m and the top of site T at 359 m can be estimated at 157.14 Ma and 160.58 Ma respectively as a first approximation. Despite 15 years of fieldwork in the area, no more sites have been discovered beneath site A or above site T. However, it does not mean that they do not exist as they may have not been exposed yet, like the newly discovered sites S and T. To date, the sites A to T can be estimated for a total of 3.44 My in duration with an average rate of 10 cm per 1000 years of sedimentation.

6. Vertical organization of seep facies

The 19 sites A to T correspond to carbonate lenses encased in marls or claystones and forming local unconformities in the Terres Noires Formation. Each site taken individually is organized as sub-vertically stacked, 2-15 m wide, lenses that are in contact (i.e., the top of an underlying lens is in sharp contact with the bottom of the overlying lens) or interbedded with marls. As for sub-site F (**Fig. 5A**), the three basal carbonate lenses, 1 to 1.5 m thick and 5 m wide, are in contact with each other and the two top carbonate lenses, 0.5 to 1 m thick and 3 m wide, are interlayered with a 0.8 to 1 m thick interval of nodule-rich marls. Sub-site F forms a 7 m high edifice composed of sub-vertically stacked carbonate lenses, lenticular in shape. The two first basal lenses are brecciated showing various-size, cemented, sub-angular clasts (**Fig. 5B**). In detail, two major types of breccia were identified:

> A matrix-supported cemented macro-breccia made up of cm to dm sub-angular and microsparite clasts within a yellowish or light brown microbial carbonate matrix.

> A dark brown cement-supported micro-breccia made up of mm to pluri-mm clasts within a slightly oil (or bitumen) impregnated matrix.

This brecciated facies is in close association with sub-vertical mineralized veins (**Fig. 5B**). The veins are filled by several generations of carbonate cement. The first generation is an iron-rich drusy calcite, 20-300 mm thick followed by bladed, high Mg-calcite or aragonite and then by 550 mm of botryoidal aragonite forming the final cement generation (***Peckman et al., 1999***). The matrix-supported cemented macro-breccia comprises clasts, the shape of which is concordant with the massive matrix of the carbonate lenses suggesting a puzzle-like structure (**Fig. 5B&C**). The dark brown cement-supported micro-breccia is more concentrated towards the veins and at some places surrounding the mineralization.

The carbonate lenses are dominated by mollusk macrofossils mostly represented by lucinid bivalves *Beauvoisina carinata* (***Gaillard et al. 1985, Rolin et al., 1990; Gaillard et al., 1992***), gastropods including *Paskentana umbilicata*, *Hokkaidoconcha novacula* (***Kiel, 2013***) and cephalopods such as ammonites (***Rolin et al., 1990***). Lucinids are usually restricted to carbonate lenses and they are not found in surrounding marls suggesting that they were endofauna. They can form dense groups with some lucinid specimens reaching 18 cm in diameter (***Rolin, 1987***). The shells provide average positive $\delta^{13}C$ values as high as +5 ‰ PDB (***Peckman et al., 1999***), probably due to symbiosis with chemosynthetic bacteria (***Rolin et al. 1990; Gaillard et al. 1992***). However, the $\delta^{13}C$ values range between -26.5 ‰ to +13 ‰ PDB in carbonate lenses (***Peckman et al., 1999***), which is consistent with the more recent values measured at site F by ***Tribovillard et al.*** (***2013***) (-18.8 ‰< $\delta^{13}C$<+12.7 ‰ PDB). In the basal lenses of site F, some lucinid specimen, 12 to 15 cm wide, were observed very close to the brecciated facies and mineralized veins (**Fig. 5C**). Some other species have been identified, such as crustacean exoskeletons, fragments and coprolites, belonging to the form-genus *Favreina* and attributed to the anomuran superfamilies *Thalassinoidea* and *Galatheoidea*, as well as fish teeth (reflecting the presence of additional predators or scavengers), sponge spicules and the irregular echinoid *Tithonia oxfordiana* (**Gaillard et al., 1985; Gaillard et al., 1992; Senowbari-Daryan et al., 2007; Kiel et al., 2010; Gaillard et al., 2011**). Probable deposit feeders, such as holothuroids (*Sclerites*), and suspension feeders, such as crinoids (ossicles), are found in minor abundance (**Gaillard et al., 2011**). Benthic foraminifers (such as *Spirillinidae*, *Nodosariidae*, *Textulariidae* and *Ophthalmidium*), ostracods, planktonic foraminifers (proto-g*lobigerinids*), radiolarians and dinoflagellates are present but less numerous. Sponges are also frequent, mainly *Lyssacid hexactinellids*, accompanied by *Lithistid* demosponges, unidentified demosponges and lychniscid hexactinellids (**Gaillard et al., 2011**). These biota are common in the Jurassic seafloor in the area suggesting a bathyal environment estimated around 600 m water depth (**Tribovillard et al, 2013)**. Ovoid to irregularly shaped fecal pellet concentrations locally scattered in the micrite indicate benthic activity (**Gaillard et al., 1985, Gaillard et al., 1992; Gaillard et al., 2011)**.

The Oxfordian seep carbonates are very rich in micritic nodules, mm to 15 cm in diameter depending on their position relative to carbonate lenses (**Fig. 5D**). These concretions formed around body fossils, such as ammonites, bivalves, spicules and any biodetritus or burrows (***Gaillard et al, 1985; Rolin, 1987***). Nodules are darker than the micritic matrix and are densely packed within the basal carbonate lenses where they form mm to 2 cm aggregates encased in a dark micrite (**Fig. 6A**). They contain framboidal pyrite, 40 to 250 mm in diameter, and are often lined by an outer rim of pyrite (***Peckman et al., 1999; Gay, 2002***). The $\delta^{13}C$ values in nodules range between -26.5 ‰ and -22.8 ‰ PDB (***Peckman et al., 1999***), with minimum values similar to the encasing carbonate lenses. They become scattered towards the margins and they can form 5 to 10 cm-long twin nodules where the carbonate lenses thin (**Fig. 6B**). Twin nodules are separated from each other over a distance between a few dm to about 1 m. These nodules appear at the same stratigraphical level as 15 cm-large nodules separated from each other by a few dm to a few meters (**Fig. 6B**). Other small nodules, 15 cm to mm in diameter can be found at the same stratigraphical level over a distance of 30 to 60 m from the centre of the carbonate lens (**Fig. 6B**). However, their diameter decreases as the distance to each other increases with distance from the carbonate lens. Beyond 60 m from the carbonate lens, they fully disappear. Bitumen is frequent within the nodules encased in marls and not in nodules encased in carbonate lenses. Other types of concretions related to sponge taphonomy and burrowing were locally described by **Gaillard et al.** (**2011**).

The carbonate lenses are composed of a micritic matrix rich in Mg-calcite, aragonite and dolomite, which are the common authigenic minerals at cold seeps (***Roberts et al. 1993***). Previous analyses conducted on marls show $\delta^{13}C$ values ranging between -19 ‰ to -17.7 ‰ far from the carbonate lenses (***Peckman et al., 1999***). These values increase close to the carbonate lenses (-0.7 ‰<$\delta^{13}C$<+1.1 ‰), which was also reported by ***Tribovillard et al. (2013)***. In addition, different types of carbonate cements were identified, such as splayed calcite, yellow calcite and botryoidal aragonite and calcite (***Beauchamp and Savard 1992***). In particular, the botryoidal fabric is presumed to be of bacterial origin (***Roberts et al. 1993***), with values of $\delta^{13}C$ between -14.8 ‰ to -12 ‰ (***Peckman et al., 1999***) reinforcing the role of microbial mediation in the building of carbonate lenses.

The top of the upper lens of many sub-sites is affected by pervasive corrosion creating vugs and irregular surfaces. Such as on top of sub-site G (**see Fig. 2 for location**), the corrosion formed a pluri-cm thick Mn- and Fe-rich crust (**Fig. 6C**), which is often associated with pyrite. Remnant pyrite-encrusted micrite nodules can be found in overlying marls for a few cm to a few dm above the oxidized crust (**Fig. 6D**).

7. Seeping sub-sites

The sub-site A is one of the more recognizable sub-seep sites of the Beauvoisin area (**See Fig. 2 for location**). It was first described as a columnar structure, different from other sub-sites B to T considered as lenticular (***Gaillard et al, 1985; Rolin, 1987***). However, the outcrop conditions with steep flanks of the Terres Noires did not give access to sub-site A until we used climbing ropes and harnesses. Sub-site A is

composed of lenticular carbonate lenses that are currently intensively eroded by present-day weathering (**Fig. 7**). All carbonate lenses that are in sharp contact with each others are considered as one unit. In consequence, 3 main units can be defined, forming sub-sites A1, A2 and A3, respectively from base to top. In terms of stratigraphic position, sub-sites A1 to A3 are Lower Oxfordian in age (**See Fig. 3 for the log correlation**), belonging to the Cordatum Zone at about 160.5 Ma (**See Fig. 4 for age estimation**). Three high-resolution stratigraphic sections were obtained in the area. Logs 1 and 2 are located respectively 60 m and 30 m south-east of the sub-sites A1 to A3, whereas log 3 follows the crest descending through the 3 sub-sites A1 to A3 (**Fig. 7**). At this scale, relevant levels 1 to 5 can be visually correlated from log to log following the general stratigraphy (S_0). Levels 1 to 4 correspond to aligned nodules following the general stratigraphy whereas level 5 is a pluri-cm thick layer of mudstone. All sections were flattened on level 5 located on top of sub-site A2 in log 3 (**Fig. 8**). The first remarkable feature is that all levels are at the same topographic level in logs 1 and 2, but levels 1 to 3 are located 4 to 6 m beneath the general stratigraphy at the base of log 3. Despite our efforts, level 4 cannot be identified in log 3 directly beneath sub-site A1. All levels, including the flat level 5, are marked by a decrease in nodule concentrations from log 3 to log 1. The number of nodules per volume of marls is markedly reduced beyond log 1 (i.e., beyond 60 m) and the nodules almost fully disappear beyond 70-80 m, e.g. at Site G (see Fig. 6).

8. Comparison with an active seep site

Sub-seeps were previously identified at the bottom of the Regab giant pockmark in the Lower Congo Basin (LCB) where a 800 m wide and 15 m deep depression at about 3150 m water depth has been documented (**Gay, 2002; Ondreas et al., 2005**). The average slope is about 2 to 3° compared to the surrounding seafloor. The detailed microbathymetry was obtained onboard the ROV-*Victor 6000* during the ZAIROV 2 and BIOZAIRE cruises in 1999-2000. The first observations show that the giant pockmark is composed of several depressions, each about 100 m wide and 6 m deep (**Ondreas et al., 2005**). In detail the small-scale depressions are not homogeneously distributed at the bottom of the pockmarks (**Fig. 9A**). The deepest two depressions are located near the centre of the Regab pockmark field. They are marked by steep flanks with an angle of about 5° compared to the horizontal plane, locally reaching 7° if compared to the regional slope whereas other small-scale depressions have smoother slopes with an angle of about 1 to 2° (**Fig. 9B**). They all have a flat bottom, meaning that they look more like a plate than a bowl structure. This is consistent with the spider structures identified at shallower depths in the Lower Congo Basin (**Casenave et al., 2017**). However, only a few concretionary carbonates have been recovered in gravity cores from the Regab giant pockmark field (**Gay et al., 2006**). This apparent lack of nodules or concretions may be due to the inability of modern coring techniques to adequately sample such carbonates (**Loyd et al., 2015**).

The studies conducted in the Regab pockmark field have shown that the highest concentrations of methane (up to 150 µl/l) in bottom waters was measured near the centre of the main depression, suggesting that this area is the actual and active methane seepage point (**Gay et al., 2006**). More precisely, a recent study

showed that only two zones are actually harboring tubeworms, mussels and clams at the same time, all living in close association with 4 m high carbonate build-ups (see Fig. 2B in **Marcon et al., 2014**), also a common feature of other giant structures such as in the Hydrate Ridge (**Teichert et al., 2005**) and in the Mediterranean Sea (**Ingrassia et al., 2015**). These two zones are annotated with green arrows on **Fig. 9B** and they correspond to the two deepest small-scale depressions identified on the dip map of the Regab pockmark field. In addition, sea-bottom pictures and videos taken within the other small-scale depressions displayed only relict features such as carbonate pavement oxidized on top and surrounding dead fauna or fields of clams on reduced black sediments (red arrows on **Fig 9B**). This may indicate a "fossil" site as remnant methane seepage (<20 µl/l) in bottom waters coupled to dead or dying fauna and oxidized crusts suggesting that fluid fluxes may have operated at higher rates in the past (**Gay et al. 2006**), as observed in other active and modern seep sites (**Greinert et al., 2001, Han et al., 2004, Haas et al., 2010**). This also suggests that only one or two points of focused fluid emission can act in a pockmark field, such as for the Hydrate Hole further North in the Lower Congo Basin (**Wenau et al., 2017**) and in other giant pockmark fields such as in the Zannnone area (**Ingrassia et al., 2015**). This is probably due to the pressure gradient allowing only one path at a time to be open as in any plumbing system (**Gay et al., 2007**).

9. Clustering of fluid venting

Predicting the pattern of gas invasion and rise in liquid-saturated sediments is still a challenge. From a theoretical point of view, the relative importance of the dominant forces in the system, i.e., buoyancy and capillary forces, have to be taken into account. The Bond (or Eötvös) number, defined as the ratio between gravity over capillarity forces, is traditionally used to characterize multiphase flow in porous media. However, this number does not account for the different spatial scales which govern the dominant forces. Indeed, the largest capillary overpressure is controlled by the narrowest space between grains ("pore neck") while the largest buoyancy force is controlled by the wider pore space ("pore body"). In order to take into account this so-called porous media aspect ratio, a modified Bond number has been introduced by **Brooks et al. (1999)**. This dimensionless parameter allows a physical classification of the flow patterns which strongly depend on the porous media aspect ratio (**Selker et al., 2007**). This latter, however, is difficult to estimate, in particular in geological settings where porosity, permeability and grain distribution may drastically change over short distances.

Laboratory experiments were therefore developed to investigate gas invasion into liquid-saturated grains in polydispersed systems. They bring the advantage of being closer to field situations, while still allowing a precise control of the imposed parameters (geometry, grain size distribution, injected gas flow-rate, and so on). These sandbox models have been used to illustrate different regimes of gas invasion in the liquid-filled granular medium (see for instance **Selker et al., 2007**, **Varas et al., 2015** and references therein): formation of gas channels, dendritic invasion, fracturing, etc. Sandbox experiments were recently conducted to investigate the temporal variations of gas emission due to gas invasion into liquid-saturated grains (**Vidal et**

al., 2010; Varas et al., 2011; Varas et al., 2015). In a 3D experiment (Fig. 10a), a constant air flow-rate (Q) is injected at the bottom of a layer of grains immersed in water. The gas is injected via a dry chamber (volume V), through a nozzle of inner diameter 1mm, localized at the bottom centre of the cell (Fig. 10a). The pressure variations in the chamber are monitored with a pressure sensor. Surface imaging makes it possible to quantify the gas emission location and dynamics. The analysis of the position of bubble emissions shows that they can migrate laterally through time (Fig. 10b). Indeed, the distance from the centre (i.e. vertical axis of the injection point, red cross in Fig.10b) varies from 0 to a few cm in any direction of the cell, for an initial grain height h_g=14cm. No specific pattern appeared at this stage, probably because grain supply simulating sedimentation has not been implemented yet in the experiment. However, two stable states of gas emission were reported during the experiment. For a significant period of time, bubbles were expelled at roughly the same position, with a minor lateral migration, defining the clusters C1 and C2 at a distance of about 2.5 and 4 cm from the centre, respectively (Fig. 10b and 10c). This study points out that, due to the strong vertical pressure gradient, gas channels cannot co-exist at the same time. In other words, only one gas channel can be active and expel gas at the surface at a given time.

10. Discussion

a) Seep site identification

The carbonate lenses of Beauvoisin were initially considered as pseudobioherms in the 80's due to their bioherm-like structure and composition (*Gaillard et al. 1985*). Although they contain reef-building organisms it is now considered that they did not form any significant relief on the seafloor (*Gaillard et al, 1985; Rolin, 1987; Peckman et al., 1999; Gay, 2002*) even if some examples on modern sites show that they can form a positive relief above the seabed (*Teichert et al., 2005; Himmler, et al., 2015*). It has been shown that carbonate pavements formed in situ into the sediments (*Bayon et al., 2009*). The presence of autochthonous biological communities, together with a high density of one or very few taxa of chemotrophic megafauna, and lateral faunal gradients, are recognizable features of seep sites (*Kauffman et al., 1996; Barbieri et al., 2005*). Moreover, the relation of fossil-rich carbonate lenses within the general stratigraphy and structural framework, their mineralogy and geochemical features, including the biomarker signatures, are indicative of chemosynthetic organism activity (*Campbell et al., 2002*). Lucinid bivalves are the most prominent biota associated with the Oxfordian carbonate lenses, with some giant specimens, up to 15-20 cm in diameter, suggesting that they fed on abundant food and nutrients (*Rolin, 1987; Gay, 2002*). Detailed paleoecology studies indicate that the communities are similar to those of recent/present hydrothermal vents and cold seeps (*Rolin et al. 1990; Gaillard et al. 1992*) and to other fossil seep sites (*Taviani, 1994; Clari et al., 1994; Taylor et al., 2009*). More recently, geochemical analyses conducted on several Beauvoisin sub-sites have led to the conclusion that they were dependent on chemosynthesis (*Peckman et al., 1999; Tribovillard et al., 2013*). The microbial oxidation of methane under anoxic conditions, referred to as sulfate-dependent anaerobic oxidation of methane (AOM), is a major biochemical

process occurring at cold seeps. At sites where AOM is active, methane concentration varies strongly depending on spatial and temporal availability of methane supply and microbial turnover rates (***Knittel and Boetius, 2009***; ***Deusner et al., 2014***). Sulfate depletion is driven by methane oxidation in sediment pore-waters through bacterially-mediated reactions, inducing a change in redox conditions (***Feng et al., 2011***) and favoring carbonate precipitation (***Bayon et al., 2007; Ge et al; 2010; Vanneste et al., 2012, and references therein***). At the Beauvoisin sub-sites the activity of sulfate-reducing bacteria is firstly indicated by the dispersively-distributed framboidal pyrite within the nodules and by an outer rim of pyrite on the nodules (***Gaillard et al. 1992; Gay, 2002***). Then, biomarkers of archaea were identified in Middle Oxfordian carbonate lenses, where methanogens produced heavy CO_2 leading to ^{13}C-enriched carbonate precipitation in the methanogenic zone with $\delta^{13}C$ values as high as +13 ‰ and 12,7 ‰ PDB (***Peckmann et al., 1999; Tribovillard et al., 2013***). The stable isotopic composition of carbonate lenses and nodules coupled with taxonomic endofauna show that all sub-sites A to T located in the Beauvoisin anticline structure can be considered as cold seeps that developed within the sediment, near to the sediment water interface in a similar fashion to modern seep sites (***Sibuet and Olu 1998, Bayon et al., 2006; Campbell et al., 2006***). This conclusion is also supported by specific enrichments in Mo, As and Sb in carbonate lenses, echoing the bacterially-mediated formation of authigenic carbonate crusts through AOM (***Tribovillard et al., 2013***) as previously shown in the modern mud-volcano of the Malta Plateau (***Cangemi et al., 2010***).

b) Spatial organization

To better understand the spatial organization of a sub-site, the centerpiece is the nodule distribution and concentration. The size, shape and spatial organization of nodules at sub-sites A1 to A3 is quite consistent with the observations made at sub-site F and G (**Fig. 6 and 8**), suggesting they have been formed through similar processes. These observations can be extended to almost all sub-sites, in spite of different outcrop conditions and forest cover. Only a few sub-sites seem not to be nodule-dependent, such as sub-sites L and M. These very close sub-sites (**See Fig. 2 for location**) mostly contain the irregular echinoid *Tithonia oxfordiana* (**Gaillard et al., 1985; Gaillard et al., 1992; Senowbari-Daryan et al., 2007; Kiel et al., 2010; Gaillard et al., 2011**) and may represent some kind of exception as they do not contain a large macrofauna either.

The general organization of a single sub-site can be summarized as a set of vertically stacked carbonate lenses located in the centre of a concentric area of nodules. The basal lens is composed of a breccia made of mineralized veins, clasts-rich conduits crosscutting limestones and embedded nodules. This facies is similar to the "brecciated limestone" from Italy (**Ladanza et al., 2013**), meaning that it may be due to an intense overpressured fluid flow impacting microbial carbonate and related macro-fauna in the sub-surface, such as what is observed in the injectite system of the Panoche Hills (**Blouet et al., 2016**). The carbonate lenses are interbedded with marls or claystones corresponding to varying fluxes of fluids such as in modern sites (**Feng et al., 2010**). The area affected by nodules is about 120 m wide forming a depression 4 to 6 m deep at a maximum compared to the regional stratigraphy as shown for sub-site A1 and A2 (**Fig. 8**

447 **and 11**). The average calculated slope is about 6°, which is visually almost undetectable in the field. Only
448 high resolution logs and the identification of marker horizons allow the identification of such low gradients.

449 ### c) Teachings from modern systems and sandbox modelling

450 Based on previous studies conducted on modern seep sites, particularly on the Regab pockmark in the LCB,
451 we have shown that the centre of an active pockmark is not the main area for focused fluid seepage and
452 the main point of emission may migrate laterally through time forming new active sub-depressions at the
453 seafloor. Consequently, a giant pockmark is the result of the coalescence of successive seepage sub-areas
454 forming a wide depression through time. This behavior is confirmed in sandbox models in which the walls
455 of a feeding channel must collapse prior to the development of a new point of emission (**Varas et al., 2015**
456 and references therein). The main consequence is an intermittent fluid seep, although the fluid supply from
457 deeper levels remains constant. This has also been documented in the Norway basin, through the Giant
458 Gjallar Vent (**Gay et al., 2012; Dumke et al., 2012**). In the light of observations made on the modern giant
459 Regab pockmark and sandbox models, an intermittent fluid seep can also be interpreted in the Beauvoisin
460 area. With respect to the stratigraphy some sub-sites can be grouped together as clusters (**Fig. 12A**). Seven
461 clusters C1 to C7 were defined in the Beauvoisin area. Except for clusters C3 and C5 containing 2 sub-sites
462 occurring at different positions at the same time, all other clusters are grouped in 200 m wide areas. It
463 means that the point of fluid emission on the seabed has remained at almost the same geographical
464 position for a significant period of time. A 3D view of the 7 clusters shows that the system shifts in time
465 from one cluster to the other (**Fig. 12B**). It also means that the occurrence of each cluster is separated from
466 the next one by a period of relative quiescence during which no fluids (or only relict fluids) were expelled at
467 the seabed. The durations of fluid seepage and fluid quiescence steps are variable. Given an estimated
468 burial of 2000-2500 m for the Terres Noires Formation in the area (***Gaillard et al., 1985; Rolin, 1987***), the
469 compaction rate at the base and bottom of the composite log can be considered equivalent. In a first
470 approximation, 7 periods of active seafloor fluid seepage and 8 periods of fluid quiescence alternated for
471 3.44 My, corresponding to periods of 200 ky each on average. However, at this stage the driving forces for
472 focused fluid migration remain unclear. Major deep-rooted faults structuring the margin during the
473 Oxfordian in the vicinity of the Beauvoisin area (in particular the Propiac fault related to halokinesis, **see**
474 **Fig. 1 for location**) may have played an efficient driving role for a long period of time, as suggested for
475 other fossil seep sites (***Aiello, 2005***). Finally, the Beauvoisin seep area can be considered as the result of
476 clustered fluid seep sub-sites. This has led to the formation of a 800 m-wide area of fluid seepage active for
477 over 3.44 My. In the light of this work, the Beauvoisin area can now be considered as a giant pockmark
478 field.

479 ### d) Evolution model

480 Based on the comparison of fossil outcrop, modern and active pockmark, and sandbox models data, we
481 propose here a new model for the internal evolution of a fluid seep area. Previous work conducted on
482 sandbox models and numerical simulations have pointed out that, independently of the initial air invasion

483 regime (percolation or fracture), similar systems develop a fluidized zone of parabolic shape characterized
484 by a central air-channel (*Varas et al., 2011; Ramos et al., 2015; Varas et al., 2015, Poryles et al., 2016*).
485 These authors show that particles are intensively reworked within the parabolic area whereas particles do
486 not have any movement outside of the parabolic area (**Fig. 13A&B**). This behavior has been previously
487 studied for hydraulic fractures showing that they can occur without tectonic stresses (*Mourgues et al.,*
488 *2011*), which is compatible with shallow unconsolidated and fluidized sediments. During the vertical growth
489 of the hydraulic fracture, representing the fluid-channelling conduit, a cone of vertical upward
490 displacements can be observed just above the tip of the fracture and the cone is limited by two large shear
491 bands, indicating that the fracture opened exclusively in pure tension mode (*Mourgues et al., 2012*). This
492 kind of cone deformation was observed in sedimentary basins, such as in the Norway basin (*Gay et al.,*
493 *2012*) or in the Northern Mediteranean Sea (*Gay et al., 2017*) where the cone structure is accompanied by
494 an uplift of the seabed suggesting that this doming is the initial phase of fluid emission preceding a general
495 collapse of the structure after which a pockmark forms. However, in the light of recent studies conducted
496 on fluid flow through a water-saturated matrix of grains, such cone structures are most probably of
497 parabolic shape (*Poryles et al., 2016*). A 2D seismic profile across the studied Regab giant pockmark field
498 shows that reflections are very chaotic below the seabed (**Fig. 13C**). The disturbed zone is in fact parabolic
499 in shape and is characterized by high amplitude reflections that were interpreted as carbonate structures
500 and/or gas-charged sediments (*Gay, 2002; Ondreas et al., 2005; Gay et al., 2006, Marcon et al., 2014*). The
501 base of the parabolic area is clearly located on top of a vertically fractured zone that is usually interpreted
502 as a seismic pipe (*Gay et al., 2006; Ho et al., 2012; Løseth et al., 2011*), very similar to the structure found
503 further North in the Lower Congo Basin at the Hydrate Hole where the deformed zone in the subsurface is
504 located right above an underlying fault clearly visible on seismic sections (*Wenau et al., 2017*). Previous
505 studies conducted in the Norway Basin have also documented V-shaped anomalies beneath pockmarks
506 corresponding to the transition from focused to distributed fluid flow (*Betzler et al., 2011; Gay et al.,*
507 *2012*). This seismic facies appears as a "flower" structure with a vertical narrow zone considered as the
508 stem (i.e. the pipe) feeding a wide area considered as the corolla (i.e. the disturbed sediments) (*Gay et al.,*
509 *2012*). It can be interpreted as deformation of cohesionless, unlithified sediments caused by fluid injection
510 (*Gay et al., 2017*).

511 We propose here a simple model of a giant fossil pockmark considered as an outcrop analogue to modern
512 giant pockmarks (**Fig. 13D**). Based on previous studies the V-shaped anomaly (*Gay et al., 2012*), or the
513 cone-in-cone structure (*Mourgues et al., 2012*), is more probably parabolic in shape. However, to date in
514 the fossil pockmark of Beauvoisin, neither the point of injection (i.e., the base of the parabolic area) nor the
515 fluid pipes were clearly identified (**Fig. 13D**). This is probably due to outcrop conditions, the Beauvoisin area
516 being located in the heart of an eroded E-W anticline structure with intense forest cover. The measured
517 values of $\delta^{13}C$ and the presence of n-alkanes in the hydrocarbon fraction of veins and nodules thus
518 correspond to a contribution of different sources of carbon including a methane thermogenic origin coming

519 from thermal maturation of organic matter at the base of the Terres Noires Formation or below it
520 (*Peckmann and Thiel, 2004*). This observation coupled with fluid migration being active for at least 3.4 My
521 suggests that a significant amount of fluids migrated during this period. However, it does not mean that the
522 fluid flow in the sub-surface is constant over time. On modern sites varying fluid flows were documented in
523 the sub-surface, producing authigenic high Mg-Calcite or aragonite depending on the CH_4 flux rate and
524 forming pavements or concretions (*Nöthen et al, 2011*). If the flux rate is not high enough, only
525 disseminated concretions precipitated. At a specific point of emission, the fluid flux in the shallow sub-
526 surface is not high enough to sustain massive carbonate precipitation, but it does not mean that the fluid
527 flux is also reduced at depth. In the disturbed zone, carbonate lenses are organized in clusters that laterally
528 migrate through time. At time t_0 the first cluster is fed by an irregular conduit (green line on **Fig. 13D**). Time
529 t_1 corresponds to the time necessary for the conduit to collapse, then to laterally shift and then to open at
530 a different location. The time t_2 corresponds to the birth of a new cluster of carbonate lenses. Based on the
531 detailed stratigraphy we showed that the times t_0, t_1 and t_2 are relatively equivalent in terms of duration,
532 about 200 ky each. It means that even if a pockmark seems dead and inactive, it could be at stage t_1
533 corresponding to a shift of the feeding conduit in the disturbed zone. As observed in both modern and
534 fossil fluid seep areas, a long lasting fluid migration is channelized through focused structures (*Ho et al.,*
535 *2012; Løseth et al., 2011*) that could constantly feed the disturbed zone. The next challenge in the area will
536 be to identify such underlying pipe structures, as the bitumen infilling of veins and nodules may correspond
537 to a later stage of heavier fluid migration as shown for the "Brecciated Limestone" in Italy (i.e., secondary
538 migration in the petroleum system; *Ladanza et al., 2015*). In the case of the Beauvoisin seep site, it would
539 mean that the feeding pipes remained open for a long period of time.

540 ## 11.Conclusion

541 For over 30 years, a fluid seep system has been known in the Beauvoisin area, located on the Jurassic
542 passive margin of the SE Basin of France (*Gaillard et al., 1985*). Modern marine investigations coupled with
543 sandbox models permitted comparison of the architecture of the Beauvoisin seep site with an active fluid
544 seep area on the modern passive margin of the Lower Congo Basin. The main conclusion is that they have
545 very similar features even if they do not occur at the same geological time. In the same way, the sandbox
546 models of fluid injection structures have shown that the involved processes have led to a similar
547 organization in 3D, in particular:

548 > **Stratigraphy:** based on 23 sedimentological sections in the Beauvoisin area, 19 sub-sites A to T have been
549 reported in a composite log, representing a total thickness of about 370 m. Due to weathering and erosion
550 since the site discovery, two new sub-sites S and T were identified and integrated in the general log, based
551 on the initial nomenclature established by *Rolin* (*1987*).

552 > **Sub-Site shape and organization:** Each identified sub-site is composed of sub-vertically stacked carbonate
553 lenses. Detailed logs at various distances from the vertical axis of carbonate lenses have shown that the

sub-sites developed in smooth depressions, 4 to 6 m deeper than the surrounding seabed. Nodules are present within the depression only. They are encased in the carbonate lenses in the centre whereas their size varies depending on the distance from the centre. Coupled with the varying $\delta^{13}C$ values, this indicates that nodules can be considered as markers of a sub-site, even if outcrop conditions do not allow identifcation of carbonate lenses buried in marls.

> **General organization:** The carbonate lenses are organized in clusters up to 7 sub-sites grouped together in the same stratigraphic interval and the same geographic zone within the seeping area. Only a few sub-sites seem active at the same time in a given cluster. The coalescence of all clusters leads to the formation of a wide depression. This general organization is very similar to that of the modern Regab giant pockmark field in the Lower Congo Basin. The seep site of Beauvoisin can be clearly considered as a fossil giant pockmark field, analogue to pockmarks in modern basins.

> **Timing:** A detailed stratigraphic correlation coupled with extensive mapping of fluid seep sub-sites in the Beauvoisin area has led to a spatio-temporal 3D reconstruction of the position of these sub-sites. It shows that periods of fluid seeping alternated with periods of apparent quiescence, about 200 ky each.

A pockmark is a seafloor depression hosting seep sites, both active and inactive. The study of the modern Regab pockmark shows that it is formed by the coalescence of smaller depressions, each about 100 m wide. However, submersible dives and gravity cores provide only the partial vision of the seafloor without integrating the sub-seafloor and the connection with fluid pipes at depth. A way to access the pockmark underground is studying outcrop analogues, such as the Beauvoisin giant pockmark. The study of this site provided a real breakthrough in the understanding of fluid activity in the disturbed zone below the seafloor. The main result is that a pockmark could seem inactive for a long period of time due to the lateral shift of the feeder conduit, meaning that the sub-seafloor remains charged in gas. This observation will be of great importance in the geobiology of fluid seeps (***Peckmann, 2005; Judd et al., 2007***), in risk assessment for anthropic activities at the sea-bottom (***Gay et al., 2017***) and for hydrocarbon exploration (***Capozzi et al., 2017***).

12.Acknowledgements

The authors would like to gratefully thank all Masters students involved in this project, Stanislas Delivet, Maëva Evesque, Laure Matiakh, Aloïse Chabbert-Gondart, Elie Boidin, Yolaine Rubert, Amandine Castillo, Charly Poitevin, Audrey Laplanche, Alexandra Gueguen and Morgane Bizeray, who helped significantly in getting stratigraphical logs. They thank Anna Travé who did all geochemical analyses at the University of Barcelona. The authors acknowledge all colleagues who participated in discussion in the field and greatly improved our understanding of the area.

13.Fundind

The field project was funded by the French coordination program Action Marge (AM). A sub-theme was dedicated to “Fluids - Organic Matter - Mineral Matter” (FO3M) and the challenge was to define fluid flow as the centerpiece of a cycle starting from the organic matter preservation at seabed, its transformation during burial forming fluids, the upward fluid migration through fine grained sediments, the temporarily fluid storage into reservoirs such as sedimentary bodies or gas hydrates, the fluid expulsion at seafloor, to its implications on seabed stability or climate change. German Varas acknowledges financial support from FONDECYT Project No. 11121300. V.V. and G.V. were supported by Programa de Cooperación Científica ECOS/CONICYT C14E07 and the Laboratoire International Associé “Matière : Structure et Dynamique” (LIA-MSD, France-Chile).

14.References

Agirrezabala, L.M., Kiel, S., Blumenberg, M., Schäfer, N., Reitner, J. (20113). Outcrop analogues of pockmarks and associated methane-seep carbonates: A case study from the Lower Cretaceous (Albian) of the Basque-Cantabrian Basin, western Pyrenees. Palaeogeography, Palaeoclimatology, Palaeoecology vol. 390, p. 94-115.

Aiello, I.W. (2005). Fossil seep structures of the Monterey Bay region and tectonic/structural controls on fluid flow in an active transform margin. Palaeogeography, Palaeoclimatology, Palaeoecology vol. 227, p. 124-142.

Aloisi, G., BOULOUBASSI I., HEIJS S.K., PANCOST R.D., PIERRE C., DAMSTE J.S.S., ... & ROUCHY J.M. (2002). - CH 4-consuming microorganisms and the formation of carbonate crusts at cold seeps. - *Earth and Planetary Science Letters*, **203**, 1, 195-203.

Aloisi, G., PIERRE C., ROUCHY J.M., FOUCHER J.P. & WOODSIDE J. (2000). - Methane-related authigenic carbonates of eastern Mediterranean Sea mud volcanoes and their possible relation to gas hydrate destabilisation. - *Earth and Planetary Science Letters*, **184**, 1, 321-338.

Amano, K., Jenkins, R.G., Aikawa, M., Nobuhara, T. (2010). A Miocene chemosynthetic community from the Ogaya Formation in Joetsu: Evidence for depth-related ecologic control among fossil seep communities in the Japan Sea back-arc basin. Palaeogeography, Palaeoclimatology, Palaeoecology vol. 286, p. 164-170.

Artru, P., 1972. Les Terres Noires du bassin rhodanien (Bajocien supérieur à Oxfordien moyen). Startigraphie - Sédimentologie - Géochimie. Thèse d'Etat, Lyon, Lyon, 173 p.

615 **Barbieri**, R., Cavalazzi, B. (2005). Microbial fabrics from Neogene cold seep carbonates, Northern Apennine,
616 Italy. Palaeogeography, Palaeoclimatology, Palaeoecology vol. 227, p. 143-155.
617 **Bayon**, G., Henderson, G.M., Bohn, M., 2009. U-Th stratigraphy of a cold seep carbonate crust. Chemical
618 Geology 260, 47–56.
619 **Bayon**, G., Pierre, C., Etoubleau, J., Voisset, M., Cauquil, E., Marsset, T., Sultan, N., Le Drezen, E., Fouquet,
620 Y., 2007. Sr/Ca and Mg/Ca ratios in Niger Delta sediments: implications for authigenic carbonate genesis in
621 cold seep environments. Marine Geology 241, 93–109.
622 **Betzler**, C., Lindhorst, S., Hübscher, C., Lüdmann, T., Fürstenau, J., Reijmer, J. (2011). Giant pockmarks in a
623 carbonate platform (Maldives, Indian Ocean). Marine Geology vol. 289, p. 1-16
624 **Blouet**, J-P., Imbert, P., Foubert, A. (2016). Mechanisms of biogenic gas migration revealed by seep
625 carbonate paragenesis, Panoche Hills, California. AAPG Bulletin vol. 101(8), p. 1309-1340.
626 **Boetius**, A., Ravenschlag, K., Schubert, C.J., Rickert, D.,Widdel, F., Gieseke,A.,Amann, R., Jorgensen, B.B.,
627 Witte, U., Pfannkuche, O., 2000. A marine microbial consortium apparently mediating anaerobic oxidation
628 of methane. Nature 407, 623–626.
629 **Bohrmann**, G., Greinert, J., Suess, E. & Torres, M. (1998). - Authigenic carbonates from the Cascadia
630 subduction zone and their relation to gas hydrate stability. - *Geology*, **26**, 7, 647-650.
631 **Brooks**, MC, Wise, WR, Annable, MD. Fundamental changes in *in-situ* air sparging flow patterns.
632 *GroundWaterMonitRem.* (1999) **19**:105–13.doi: 10.1111/j.1745-6592.1999.tb00211.x
633 **Campbell**, K.A. (2006). Hydrocarbon seep and hydrothermal vent paleoenvironments and paleontology:
634 past developments and future research directions. Palaeogeography, Palaeoclimatology, Palaeoecology vol.
635 232, p. 362-407.
636 **Campbell**, K.A., Farmer, J.D., Des Marais, D. (2002). Ancient hydrocarbon seeps from the Mesozoic
637 convergent margin of California: carbonate geochemistry, fluids and palaeoenvironments. Geofluids vol. 2,
638 p. 63-94.
639 **Campbell**, K.A., and Bottjer, D.J. (1995b). Peregrinella: an Early Cretaceous cold-seep-restricted brachiopod.
640 Paleobiology vol. 24, p. 461-478.
641 **Campbell**, K.A., Bottjer, D.J. (1995a). Brachiopods and chemosymbiotic bivalves in Phanerozoic
642 hydrothermal vent and cold seep environments. Geology vol. 23, p. 321-324.

643 **Cangemi**, M., Di Leonardo, R., Bellanca, A., Cundy, A., Neri, R., Angelone, M., 2010. Geochemistry and
644 mineralogy of sediments and authigenic carbonates from the Malta Plateau, Strait of Sicily (Central
645 Mediterranean): relationships with mud/fluid release from a mud volcano system. Chemical Geology 276,
646 294–308.
647 **Capozzi**, R., Oppo, D., Taviani, M. (2017). Cold seepages: An economic tool for hydrocarbon appraisal. AAPG
648 Bulletin vol. 101(4), p. 617-623.
649 **Casenave**, V., Gay, A., Imbert, P. (2017). Spider structures: records of fluid venting from methane hydrates
650 on the Congo continental slope. Bulletin de la Société Géologique de France 188 (4), E3.
651 **Clari**, P., Fornara, L., Ricci, B., Zuppi, G.M. (1994). Methane-derived carbonates and chemosymbiotic
652 communities of Piedmont (Miocene, northern Italy): an update. Geo-Marine Letters vol. 14, p. 201-209.
653 **Claypool**, G.E., Holser, W.T., Kaplan, I.R., Sakai, H., Zak, I., 1980. The age curves of sulphur and oxygen
654 isotopes in marine sulphate and their interpretation. Chemical Geology (Isotope geoscience section) 28,
655 199-260.
656 **Craig**, H., Gordon, I., 1965. Deuterium and oxygen-18 variations in the ocean and marine atmosphere. In:
657 Tongiorgi, E. (Ed.), Stable Isotopes in Oceanographic Studies and Paleotemeratures. Consiglio Nazionale
658 delle Richerche, Laboratorio di Geologia Nucleare, Pisa, Italy. 9-130.
659 **Dardeau**, G., 1988. Tethyan evolution and Alpine reactivation of Jurassic extensional structures in the
660 French "Alpes Maritimes". Bulletin de la Société Géologique de France, Vol. 8(No. 4): p. 651-657.
661 **Deusner**, C., Holler, T., Arnold, G.L., Bernasconi, S.M., Formolo, M.J., Brunner, B. (2014). Sulfur and oxygen
662 isotope fractionation during sulfate reduction coupled to anaerobic oxidation of methane is dependent on
663 methane concentration. Earth and Planetary Science Letters ,399, p. 61-73.
664 Dumke, I., Berndt, C., Crutchley, G.J., Krause, S., Liebetrau, V., **Gay, A.**, Couillard, M., (2014). Seal bypass at
665 the Giant Gjallar Vent (Norwegian Sea): Indications for a new phase of fluid venting at a 56-Ma-old fluid
666 migration system. Marine Geology 351, p. 38-52.
667 **Feng**, D., CHEN D., PECKMANN J. & BOHRMANN G. (2010). - Authigenic carbonates from methane seeps of
668 the northern Congo fan: microbial formation mechanism. - *Marine and Petroleum Geology*, **27**, 4, 748-756.
669 **Feng**, D., Roberts, H.H. (2011). Geochemical characteristics of the barite deposits at cold seeps from the
670 northern Gulf of Mexico continental slope. Earth and Planetary Science Letters vol. 309, p. 89-99.

671 **Gaillard**, C., Neraudeau D., and Thierry J. 2011. *Tithonia oxfordiana*, a new irregular echinoid associated
672 with Jurassic seep deposits in South-East France. Palaeontology, 54:735–752.
673 **Gaillard**, C., Atrops, F., Marchand, D., Hanzo, M., Lathuilière, B., Bodeur, Y., Ruget, C., Nicollin, J-P., Werner,
674 W. (1996). Description stratigraphique préliminaire des faisceaux alternants de l'Oxfordien moyen dans le
675 bassin dauphinois (Sud-Est de la France). Géologie de la France vol. 1, p. 17-24.
676 **Gaillard**, C., Rio, M., Rolin, Y., Roux, M. 1992. Fossil chemosynthetic communities related to vents or seeps
677 in sedimentary basins: the pseudobioherms of southeastern France compared to other world examples.
678 Palaios, 7, 451–465.
679 **Gaillard**, C., Bourseau, J.-P., Boudeulle, M., Pailleret, P., Rio, M., Roux, M. 1985. Les pseudobiohermes de
680 Beauvoisin (Drôme): un site hydrothermal sur la marge téthysienne à l'Oxfordien ? Bulletin de la Société
681 Géologique de France vol. 1, 69–78.
682 **Gaillard**, C., Rolin, Y., 1988. Relation entre tectonique synsédimentaire et pseudobiohermes (Oxfordien de
683 Beauvoisin-Drôme-France). Un argument supplémentaire pour interpréter les pseudobiohermes comme
684 formés au droit de sources sous-marines. Comptes Rendus Académie des Sciences Paris 307, 1265–1270.
685 **Gaillard**, C., Bourseau, J.P., Boudeulle, M., Pailleret, P., Rio, M., Roux, M., 1985. Les pseudobiohermes de
686 Beauvoisin (Drôme): un site hydrothermal sur la marge téthysienne l'Oxfordien? Bulletin de la Société
687 Géologique de France, série 8 1, 69–78.
688 **Gay**, A., Migeon, S. (2017). Geological fluid flow in sedimentary basins. Bulletin de la Société Géologique de
689 France vol. 188(E3), p. 1-6. DOI:10.1051/bsgf/2017200
690 **Gay**, A., Cavailhes, T., Grauls, D., Marsset, B., Marsset, T., 2017. Repeated fluid expulsions during events of
691 rapid sea-level rise in the Gulf of Lion, western Mediterranean Sea. Bulletin de la Société Géologique de
692 France vol. 188, 24 DOI: 10.1051/bsgf/2017190
693 **Gay**, A., Mourgues, R., Berndt, C., Bureau, D., Planke, S., Laurent, D., Gautier, S., Lauer, C. and Loggia, D.
694 (2012). Anatomy of a fluid pipe in the Norway Basin: initiation, propagation and 3D shape. Marine Geology.
695 **Gay**, A., Lopez, M., Berndt, C. and Séranne, M., (2007). Geological controls on focused fluid flow associated
696 with seafloor seeps in the Lower Congo Basin. *Marine Geology*, 244: 68-92.
697 **Gay**, A., M. Lopez, H. Ondreas, J.-L. Charlou, G. Sermondadaz & P. Cochonat (2006). Seafloor facies related
698 to upward methane flux within a Giant Pockmark of the Lower Congo Basin. *Marine Geology*. 226, 81-95.

Gay, A., 2002. Les marqueurs géologiques de la migration et de l'expulsion des fluides sédimentaires sur le plancher des marges passives matures. Exemples dans le Bassin du Congo. Thèse Université de Lille 1, 426 pp.

Ge, L., Jiang, S.-Y., Swennen, R., Yang, T., Yang, J.-H., Wu, N.-Y., Liu, J., Chen, D.H., 2010. Chemical environment of cold seep carbonate formation on the northern continental slope of South China Sea: Evidence from trace and rare earth element geochemistry. Marine Geology 277, 21–30.

Gradstein, J.G., "The Geologic Time Scale 2012" by, J.G. Ogg, M.D. Schmitz and G.M. Ogg (Elsevier, 2012).

Greinert, J., Bohrmann, G. & Suess, E. (2001). - Gas hydrate-associated carbonates and methane-venting at Hydrate Ridge: classification, distribution and origin of authigenic lithologies. - *Geophysical Monograph-American Geophysical Union*, **124**, 99-114.

Han, X., Suess, E., Sahling, H. & Wallmann, K. (2004). - Fluid venting activity on the Costa Rica margin: new results from authigenic carbonates. - *International Journal of Earth Sciences*, **93**, 4, 596-611.

Haas, A., Peckmann, J., Elvert, M., Sahling, H. & Bohrmann, G. (2010). - Patterns of carbonate authigenesis at the Kouilou pockmarks on the Congo deep-sea fan. - *Marine Geology*, **268**, 1, 129-136.

Himmler, T., Birgel, D., Bayon, G., Pape, T., Ge, L., Bohrmann, G., Peckmann, J. (2015). Formation of seep carbonates along the Makran convergent margin, northern Arabian Sea and a molecular and isotopic approach to constrain the carbon isotopic composition of parent methane. Chemical Geology vol. 415, p. 102-117.

Ho, S., Cartwright, J.A., Imbert, P. (2012). Vertical evolution of fluid venting structures in relation to gas flux, in the Neogene-Quaternary of the Lower Congo Basin, Offshore Angola. Marine Geology vol. 332, p. 40-55.

Ingrassia, M., Martorelli, E., Bosman, A., Macelloni, L., Sposato, A., Chiocci, F.L. (2015). The Zannone Giant Pockmark: First evidence of a giant complex seeping structure in shallow-water, central Mediterranean Sea, Italy. Marine Geology vol. 363, p. 38-51.

Judd, A. & Hovland, M. (2007). - Seabed Fluid Flow, the Impact on Geology, Biology and the Marine Environment. - Cambridge University Press, Statoil Norway, 290-314.

Kauffman, E.G., Arthur, M.A., Howe, B., Scholle, P.A. (1996). Widespread venting of methane-rich fluids in Late Cretaceous (Campanian) submarine springs (Tepee Buttes), Western Interior seaway, U.S.A. Geology, vol. 24(9), p. 799-802.

727 **Kiel**, S. (2013). Lucind bivalves from ancient methane seeps. Journal of Molluscan Studies 79: 346–363.
728 doi:10.1093/mollus/eyt035
729 **Kiel**, S. (2010). The fossil record of vent and seep mollusks. In The Vent and Seep Biota: Aspects from
730 Microbes to Ecosystems (Ed. S. Kiel), PP. 255-278. Topics in Geobiology vol. 33. Heidelberg: Springer.
731 **Kiel**, S., & Little, C.T.S. (2006). Cold seep mollusks are older than the general marine mollusk fauna. Science
732 vol. 313, P. 1429-1431.
733 **Knittel**, K. & Boetius, A. (2009). Anaerobic oxidation of methane: progress with an unknown process.
734 Annual Review of Microbiology, vol. 63, p. 311-344.
735 **Ladanza**, A., Sampalmieri, G., Cipollari, P. (2015). Deep-seated hydrocarbons in the seep "Brecciated
736 Limestones" of the Maiella area (Adriatic foreland basin): Evaporitic sealing and oil re-mobilization effects
737 linked to the drawdown of the Messinian Salinity Crisis. Marine and Petroleum Geology vol. 66, p. 177-191.
738 **Ladanza**, A., Sampalmieri, G., Cipollari, P., Mola, M., Cosentino, D. (2013). The "Brecciated Limestones" of
739 Maiella, Italy: Rheological implications of hydrocarbon-charged fluid migration in the Messinian
740 Mediterranean Basin. Palaeogeography, Palaeoclimatology, Palaeoecology vol. 390, p. 130-147.
741 **Lemoine**, M. (1985). Structuration jurassique des Alpes occidentales et palinspatique de la Téthys ligure.
742 Bulletin de la Société Géologique de France vol. I(1), p. 126-137. DOI:10.2113/gssgfbull.I.1.127
743 **Lemoine**, M., Arnaud-Vanneau, A., Arnaud, H., Létolle, R., Mével, C., Thieuloy, J.P. (1982). Indices possibles
744 de paléo-hydrothermalisme marin dans le Jurassique et le Crétacé des Alpes occidentales (océan téthysien
745 et sa marge continentale européenne): essai d'inventaire. Bulletin de la Société Géologique de France vol.
746 S7-XXIV (3), p. 641-647. DOI: 10.2113/gssgfbull.S7-XXIV.3.641
747 **Løseth**, H. et al., 2011. 1000 m long gas blow-out pipes. Marine and Petroleum Geology, 28: 1047-1060.
748 **Louis-Schmid**, B., Rais, P., Logvinovich, D., Bernasconi, S.M., Weissert, H. (2007). Impact of methane seeps
749 on the local carbon-isotope record: a case study from a Late Jurassic hemipelagic section. Terra Nova vol.
750 19(4), p. 259-265.
751 **Loyd**, S.J., Berelson, W.M. (2015). The modern record of "concretionary" carbonate: Reassessing a
752 discrepancy between modern sediments and the geologic record. Chemical Geology vol. 420, p. 77-87.
753 **Marcon**, Y., Ondréas, H., Sahling, H., Bohrmann, G., Olu, K. (2014). Fluid flow regimes and growth of a giant
754 pockmark. Geology, Vol. 42(No. 1), p. 63-66.

Mascle, G. *et al.*, 1988. Salt tectonics, Tethyan rifting and Alpine folding in the French Alps. Bulletin de la Société Géologique de France, Vol. 8(No. 4): p. 747-758.

Mourgues, R., Bureau, D., Bodet, L., Gay, A. and Gressier, J., 2012. Formation of conical fractures in sedimentary basins: Experiments involving pore fluids and implications for sandstone intrusion mechanisms. Earth and Planetary Science Letters, 313: 67-78.

Mourgues, R., Gressier, J.B., Bodet, L., Bureau, D. and Gay, A., 2011. "Basin scale" versus "localized" pore pressure/stress coupling: Implications for trap integrity evaluation. Marine and Petroleum Geology, 28(5): 1111-1121.

Natalicchio, M., Peckmann, J., Birgel, D. & Kiel, S. (2015). Seep deposits from northern Istria, Croatia: a first glimpse into the Eocene seep fauna of the Tethys region. Geology Magazine vol 152 (3), p. 444-459.

Ondreas, H., J-L. Charlou, K. Olu, Y. Fouquet, P. Cochonat, *A. Gay,* B. Dennielou, J. P. Donval, A. Fifis, T. Nadalig, & M. Sibuet. (2005) Integrated "in situ" study of a deep giant pockmark on the Congo-Angola margin. *Geo-Marine Letters*. 25, 281-292.

Paull, C.K., Chanton, J.P., Neumann, A.C., Coston, J.A. & Martens, C.S. (1992). - Indicators of methane-derived carbonates and chemosynthetic organic carbon deposits: examples from the Florida escarpment. *In*: Beauchamp, B. & Von Bitter, P., Eds., Chemosynthesis: Geological Processes and Products. - *Soc. Econ. Paleontol. Mineral.*, 361–375.

Peckmann, J. (2005). Geobiology of ancient and modern methane seeps. Palaeogeography, Palaeoclimatology, Palaeoecology vol. 227, p. 1-5.

Peckmann J. & Thiel, V. (2004). - Carbon cycling at ancient methane–seeps. - *Chemical Geology*, **205**, 3, 443-467.

Peckmann, J., Thiel, V., Michaelis, W., Clari, P., Gaillard, C., Martire, L., & Reitner, J. (1999). Cold seep deposits of Beauvoisin (Oxfordian; southeastern France) and Marmorito (Miocene; northern Italy): microbially induced authigenic carbonates. International Journal of Earth Sciences vol 88, p. 60-75.

Pellenard, P., Deconinck, J.F., Huff, W.D., Thierry, J., Marchand, D., Trouiller, A. 2003. Characterisation and correlation of Upper Jurassic (Oxfordian) bentonite deposits of the Paris Basin and the South-Eastern Basin of France. Sedimentology, 50, 6, 1035-1060 (A2)

Pellenard, P., Deconinck, J.F., Marchand, D., Thierry, J., Fortwengler, D., Vigneron, G., 1999. Contrôle géodynamique de la sédimentation argileuse du Callovien-Oxfordien moyen dans l'Est du Bassin de Paris : influence eustatique et volcanique. C.R. Acad. Sci. Paris, 328, 807-813 (A1).

Poryles, R., Vidal, V., Varas, G. (2016). Bubbles trapped in a fluidized bed: trajectories and contact area. Physical Review E93, 032904.

Rolin, Y., Gaillard, C., Roux, M. (1990). Ecologie des pseudobiohermes des Terres Noires jurassiques liés à des paléo-sources sous-marines. Le site oxfordien de Beauvoisin (Drôme, Bassin du Sud-Est, France). Paleogeography, Palaeoclimatology, Palaeoecology, vol. 80, p. 79-105.

Rolin, Y. (1987). Gisements fossilifères liés à des sources sous-marines dans le bassin des Terres Noires: le site oxfordien de Beauvoisin (Drôme, Chaînes subalpines méridionales), Comparaison avec les sites océaniques actuels. Thèse de doctorat Lyon, 128 p.

Ramos, G., G. Varas, J.-C. G´eminard, and V. Vidal, Gas-induced fluidization of mobile liquid-saturated grains, Phys. Rev. E **92**, 062210 (2015).

Selker, JS, Niemet, M, McDuffie, NG, Gorelick, SM, Parlange, JY. The local geometry of gas injection into saturated homogeneous porous media. *TranspPorousMed.* (2007) **68**:107–27.doi:10.1007/s11242-006-0005-0

Senowbari-Daryan, B., Gaillard, C., Peckmann, J. (2007). Crustacean microprolites from Jurassic (Oxfordian) hydrocarbon-seep deposits of Beauvoisin, southeastern France. Facies vol. 53, p. 229-238.

Stewart, S.A. (2015). Circular geological structures outcropping in the sedimentary basins of Saudi Arabia. Journal of Asian Earth Sciences vol. 106, p. 95-118.

Taviani, M. (1994). The "calcari a Lucina" macrofauna reconsidered: Deep-sea faunal oases from Miocene-age cold vents in the Romagna Apennine, Italy. Geo-Marine Letters vol. 14, p. 185-191.

Taylor, J.D., Glover, E.A. (2009). A giant lucinid bivalve from the Eocene of Jamaica - Systematics, life habits and chemosymbiosis (Mollusca: bivalvia: Lucinidae). Palaeontology vol. 52, Part 1, p. 95-109.

Teichert B.M.A. van de Schootbrugge B. (Ed.): 2013. *Tracing Phanerozoic hydrocarbon seepage from local basins to the global Earth system*. : Elsevier. doi: 10.1016/j.palaeo.2013.10.001.

Teichert, B.M.A., Bohrmann, G., Suess, E. (2005). Chemoherms on Hydrate Ridge - Unique microbially-mediated carbonate build-ups growing into the water column. Palaeogeography, Palaeoclimatology, Palaeoecology vol. 227, p. 67-85.

Tribovillard, N., Armynot du Châtelet, E., Gay, A., Barbecot, F., Sansjofre, P. and Potdevin, J-L., 2013. Geochemistry of cold seepage-impacted sediments: per-ascensum or per-descensum trace metal enrichment ?. Chemical Geology vol. 340, p. 1-12.

Vanneste, H., Kastner, M., James, R.H., Connelly, D.G., Fisher, R.E., Kelly-Gerreyn, B.A., Heeschen, K., Haeckel, M., Mills, R.A., 2012. Authigenic carbonates from the Darwin Mud Volcano, Gulf of Cadiz: a record of palaeo-seepage of hydrocarbon bearing fluids. Chemical Geology 300–301, 24–39.

Varas, G., V. Vidal, and J.-C. Géminard, Venting dynamics of an immersed granular layer, Phys. Rev. E **83**, 011302 (2011).

G. Varas, G. Ramos, J.-C. Géminard, and V. Vidal, Flow and fracture in water-saturated, unconstrained granular beds, Front. Phys. **3**, 44 (2015).

Vidal, V., Varas, G, Géminard, J-C. (2010). Dynamique de dégazage dans un milieu granulaire immergé : différents aspects. Compte-rendus de la 13e Rencontre du Non-Linéaire, Eds. C. Josserand, M. Lefranc & C. Letellier, Non-Linéaire Publications, p.199-204.

Vidal, V., Varas, G, Géminard, J-C. (2011). `Venting' dans un milieu granulaire immergé. Compte-rendus de la 14e Rencontre du Non-Linéaire, Eds. C. Josserand, M. Lefranc & C. Letellier, Non-Linéaire Publications, p.175-180

Vrijenhoeck, R.C. (2013). On the instability and evolutionary age of deep-sea chemosynthetic communities. Deep-Sea Research II vol. 92, p. 189-200.

Wenau, S., Spieβ, V., Pape, T., Fekete, N. (2017). Controlling mechanisms of giant deep water pockmarks in the Lower Congo Basin. Marine and Petroleum Geology vol. 83, p. 140-157.

Whiticar M. J. (1999). - Carbon and hydrogen isotope systematics of bacterial formation and oxidation of methane. - *Chemical Geology*, **161**, 1, 291-314.

List of figures

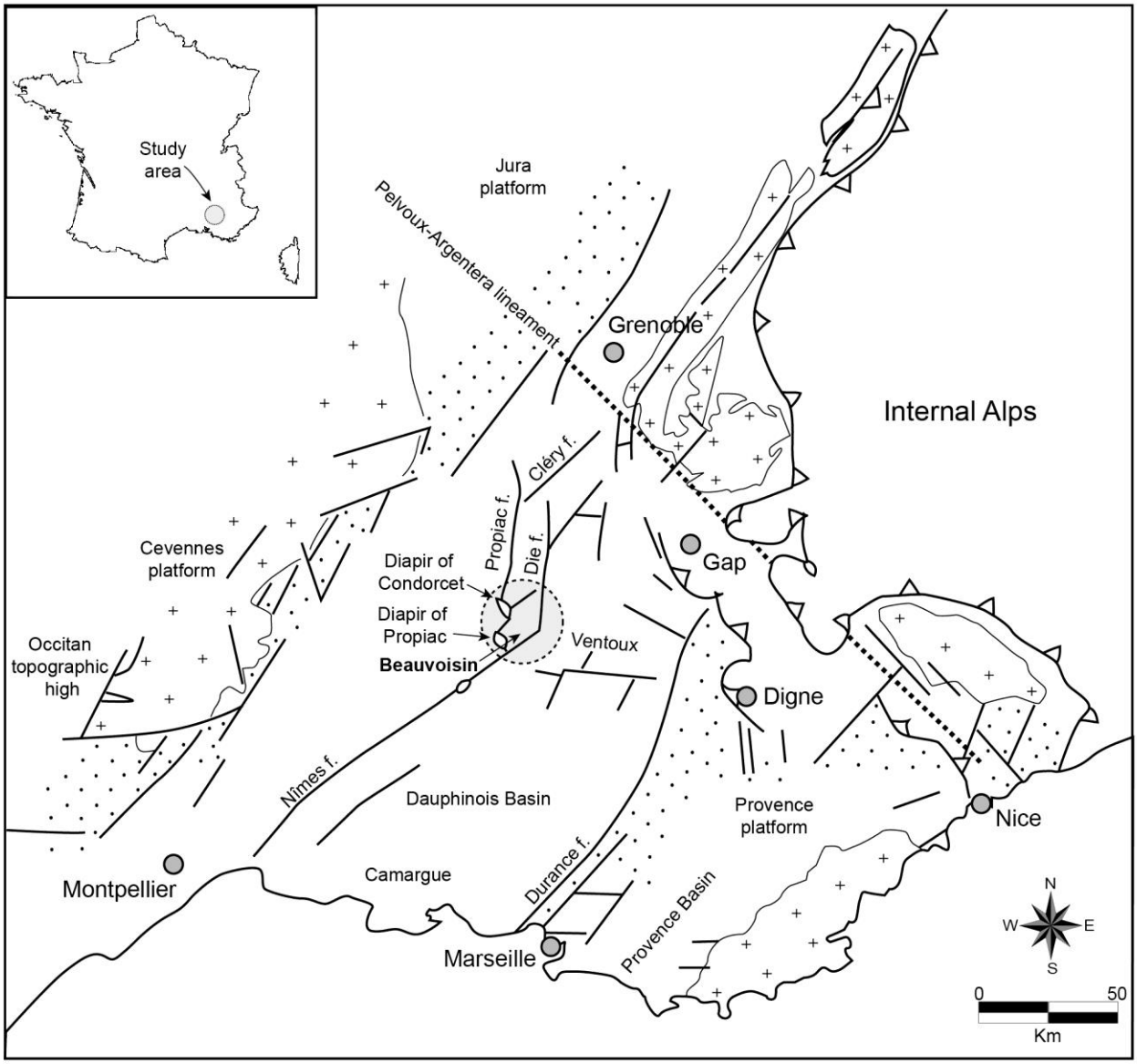

835

836 ***Figure 1: Simplified structural map of the South East Basin of France. The study area is located between the Propiac***

837 ***Fault and the Die Fault north of the Ventoux in a relay zone corresponding to the heritage of syn-sedimentary faults***

838 ***that structured the Jurassic Tethyian margin. In the Beauvoisin area (grey circle on the map) the identified seep sites***

839 ***developed in dark marls called the "Terres Noires" Formation (Oxfordian).***

840

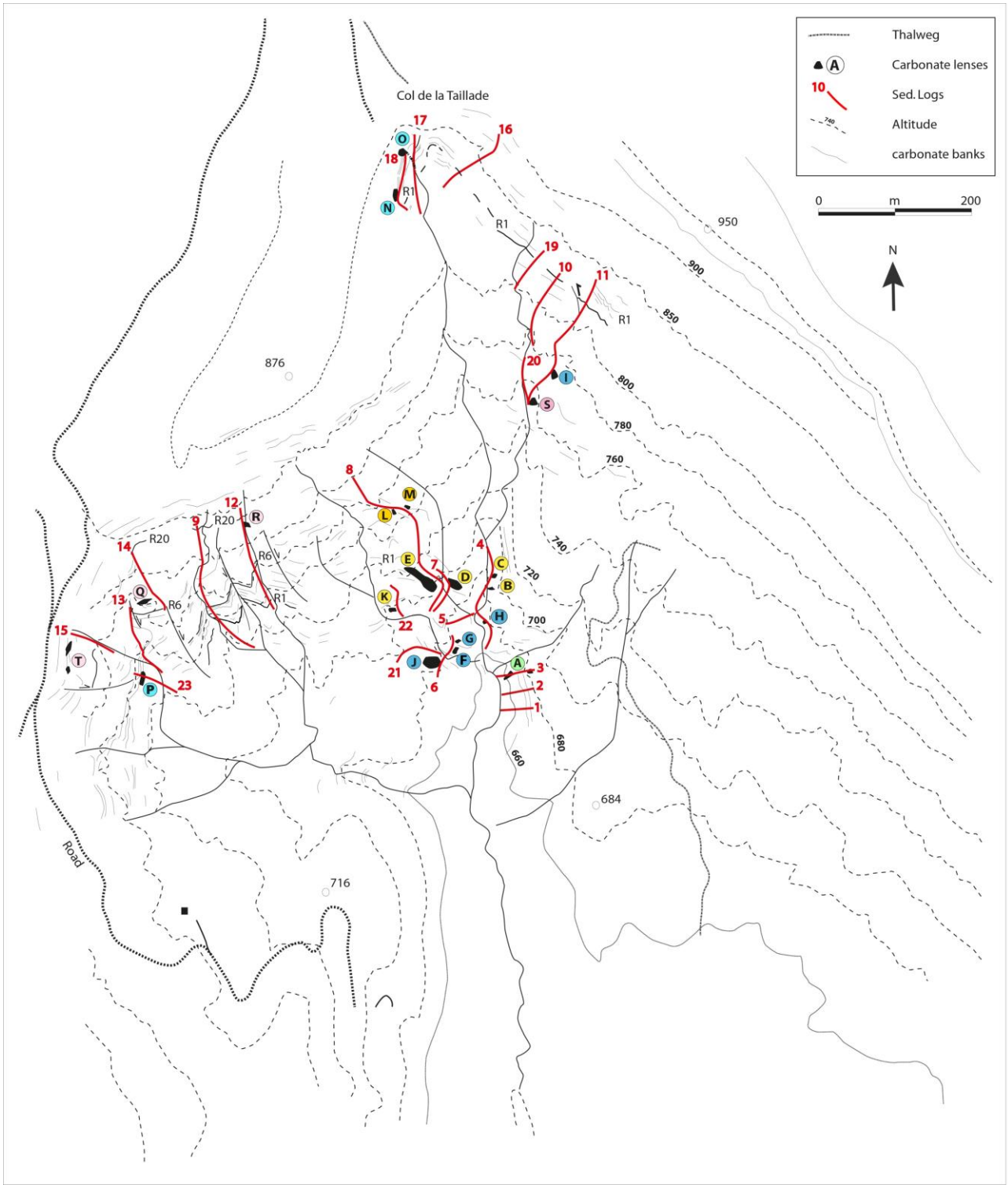

841

842 ***Figure 2:Detailed topographic map of the Beauvoisin area (modified after Gaillard et al., 1985). 23 sedimentological***

843 ***logs have been recovered (red lines) between 2002 and 2016 in steep valleys. Almost all valleys have been explored,***

844 ***depending on safety conditions. 19 sub-sites have been reported, including two new sites, S and T, that were***

845 ***exposed due to weathering since the initial mapping.***

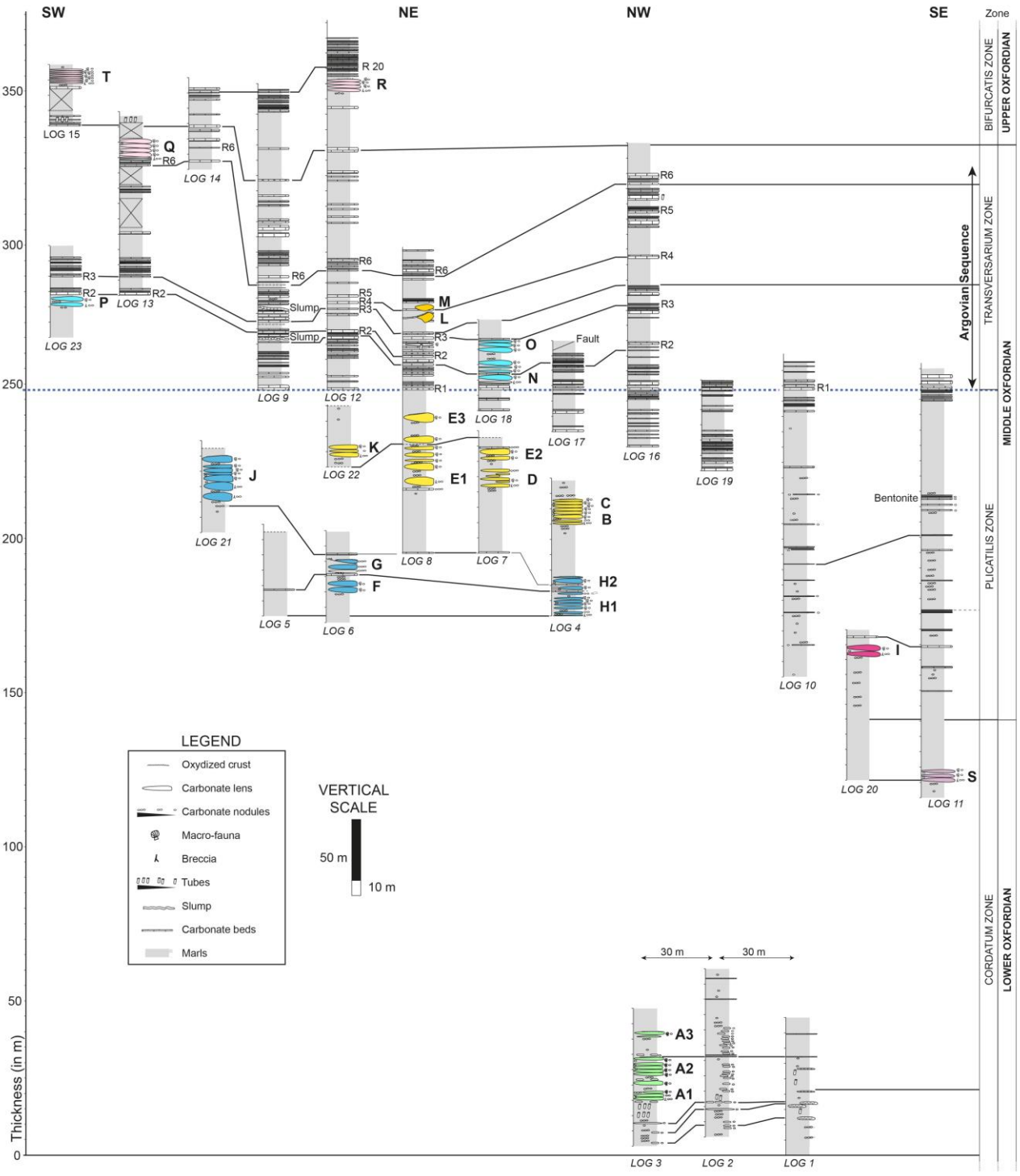

846

847 ***Figure 3: Correlation of the 23 sedimentological logs in the Beauvoisin area regarding the general stratigraphy of***
848 ***the Oxfordian. The 23 stratigraphical logs were obtained utilising key marker layers, R1 to R20 following the***
849 ***nomenclature of Gaillard et al. (1985) and Rolin (1987). The correlation is centered and flattened on the R1 level***
850 ***corresponding to the base of the Argovian sequence ending on top with the R6 level.***

851

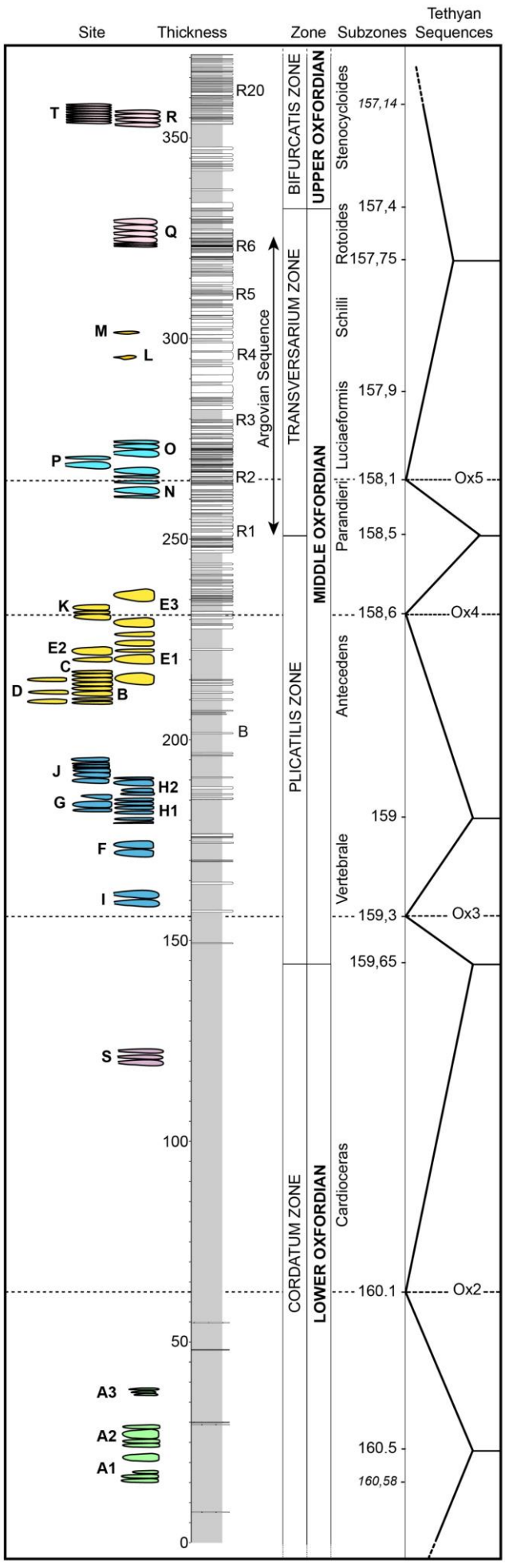
Site
Thickness
Zone
Subzones
Tethyan Sequences
T
R
Q
M
L
P
O
N
K
E3
E2
E1
C
D
B
J
H2
G
H1
F
I
S
A3
A2
A1
R20
R6
R5
R4
R3
R2
R1
Argovian Sequence
350
300
250
200
150
100
50
0
BIFURCATIS ZONE
TRANSVERSARIUM ZONE
PLICATILIS ZONE
CORDATUM ZONE
UPPER OXFORDIAN
MIDDLE OXFORDIAN
LOWER OXFORDIAN
Stenocycloides
Rotoides
Schilli
Luciaeformis
Parandieri
Antecedens
Vertebrale
Cardioceras
157,14
157,4
157,75
157,9
158,1
158,5
158,6
159
159,3
159,65
160.1
160.5
160,58
Ox5
Ox4
Ox3
Ox2

Figure 4: Composite log of the Oxfordian in the Beauvoisin area taking into account eroded missing sequences, slump deposits and faults (360 m in thickness). The oldest site A is located within the Cordatum Zone (Lower Oxfordian) whereas the youngest site T is in the Bifurcatis Zone (Upper Oxfordian) according to the Tethysian sequences and age model from Gradstein et al. (2012) .

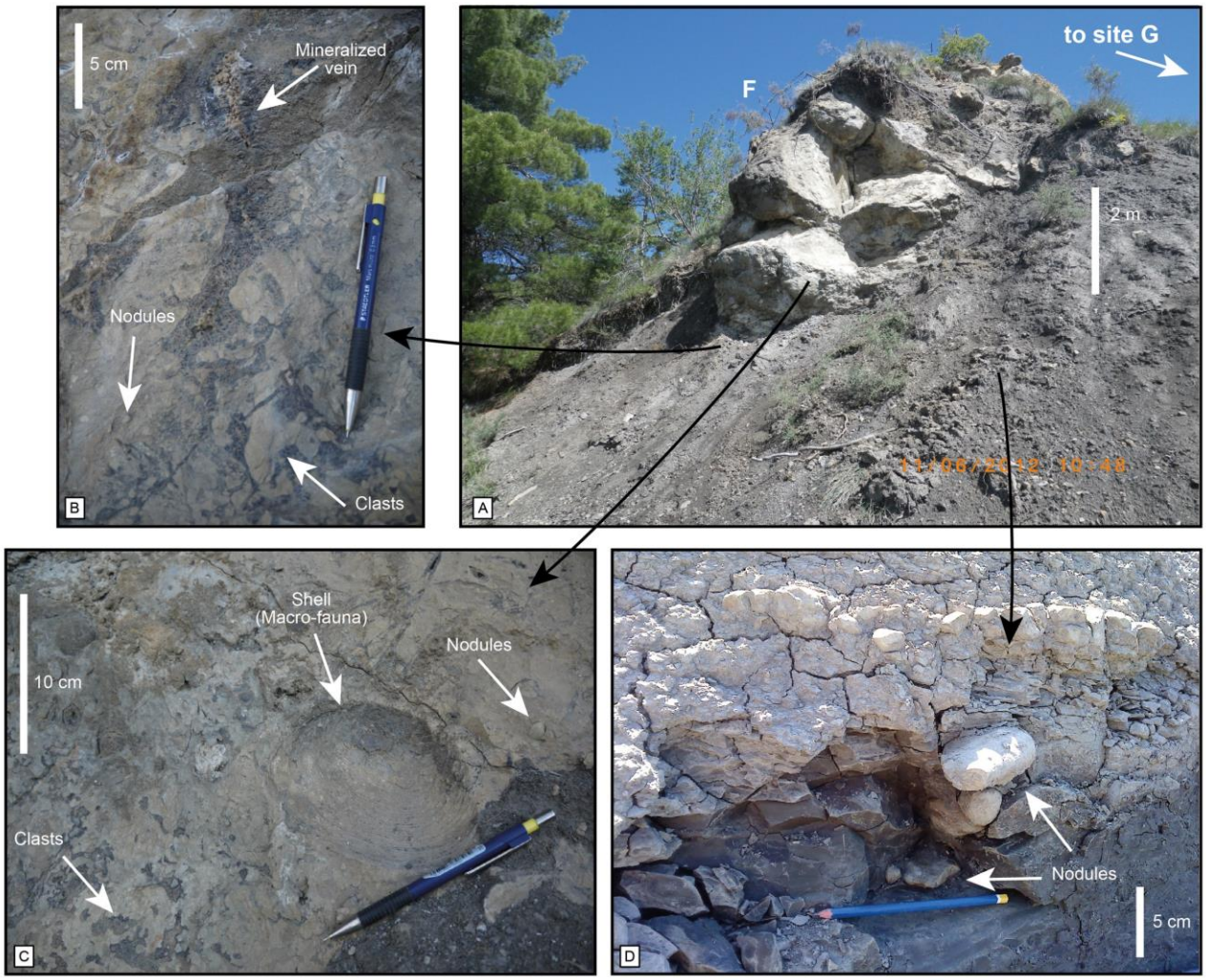

Figure 5: Sub-site F located in the centre of the Beauvoisin area (See Fig. 2 for location). A) View to the West of site F forming a 7 m high edifice composed of sub-vertically stacked carbonate lenses. B) Detailed photograph of the basal carbonate lens showing the brecciated facies dominated by sub-vertical veins yielding mineralizations and displaying a puzzle-like structure. C) Detailed photograph showing lucinid specimen, 12 to 15 cm wide, in close association with the brecciated facies and mineralized veins. D) Detailed photograph showing micritic nodules, mm to 15 cm in diameter.

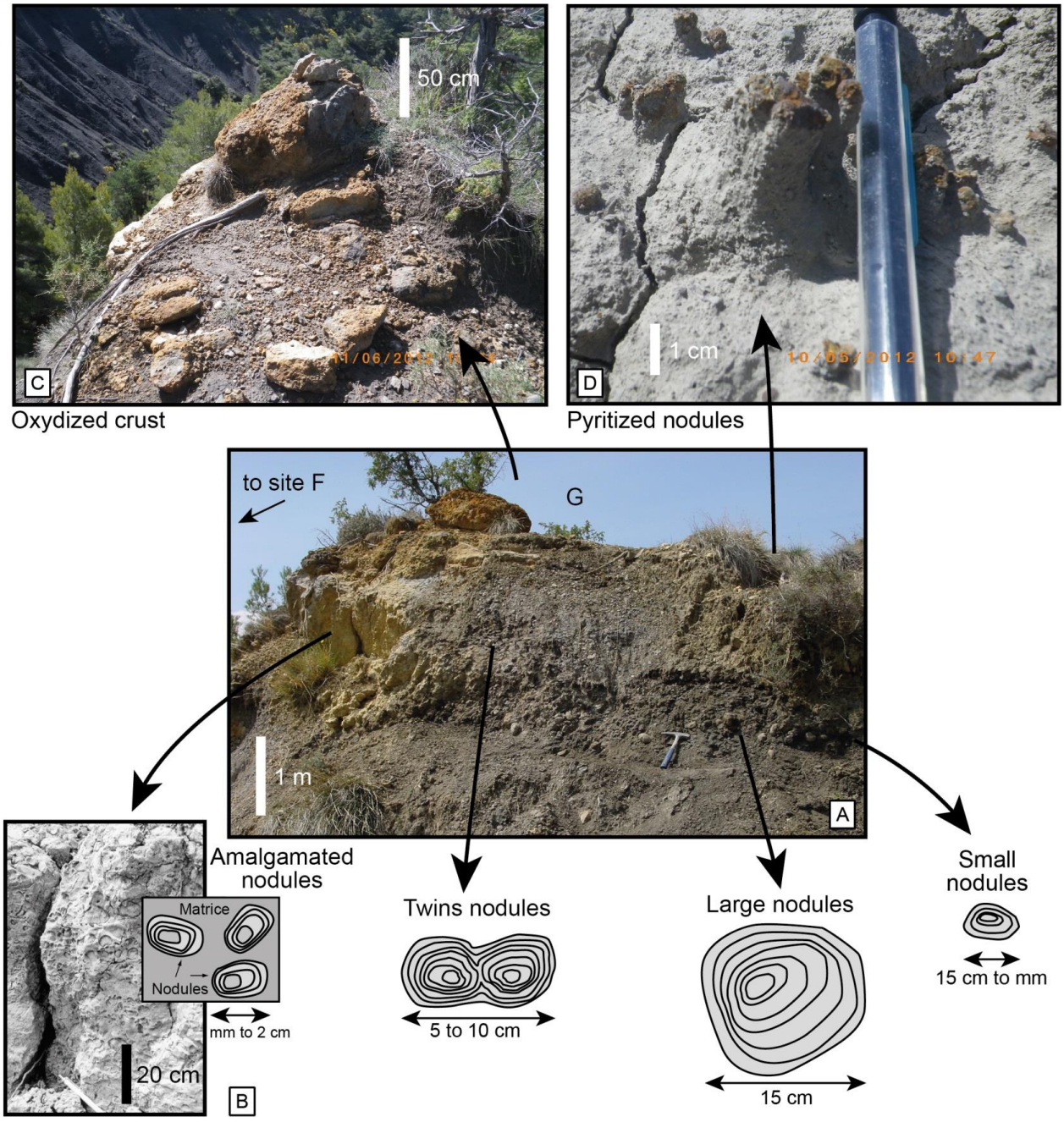

Figure 6: Sub-site G located in the centre of the Beauvoisin area and just above the sub-site F (See Fig. 2 for location). A) Outcrop photograph showing densely packed mm to 2 cm aggregates nodules encased in a dark micrite within the basal carbonate lenses. B) Organization and shape of nodules depending on their distance to the carbonate lens. C) Photograph of the top of sub-site G showing corrosion forming a pluri-cm thick Mn and Fe rich crust. D) Detailed photograph showing pyrite-encrusted micrite nodules overlying marls for a few cm to a few dm above the oxidized crust.

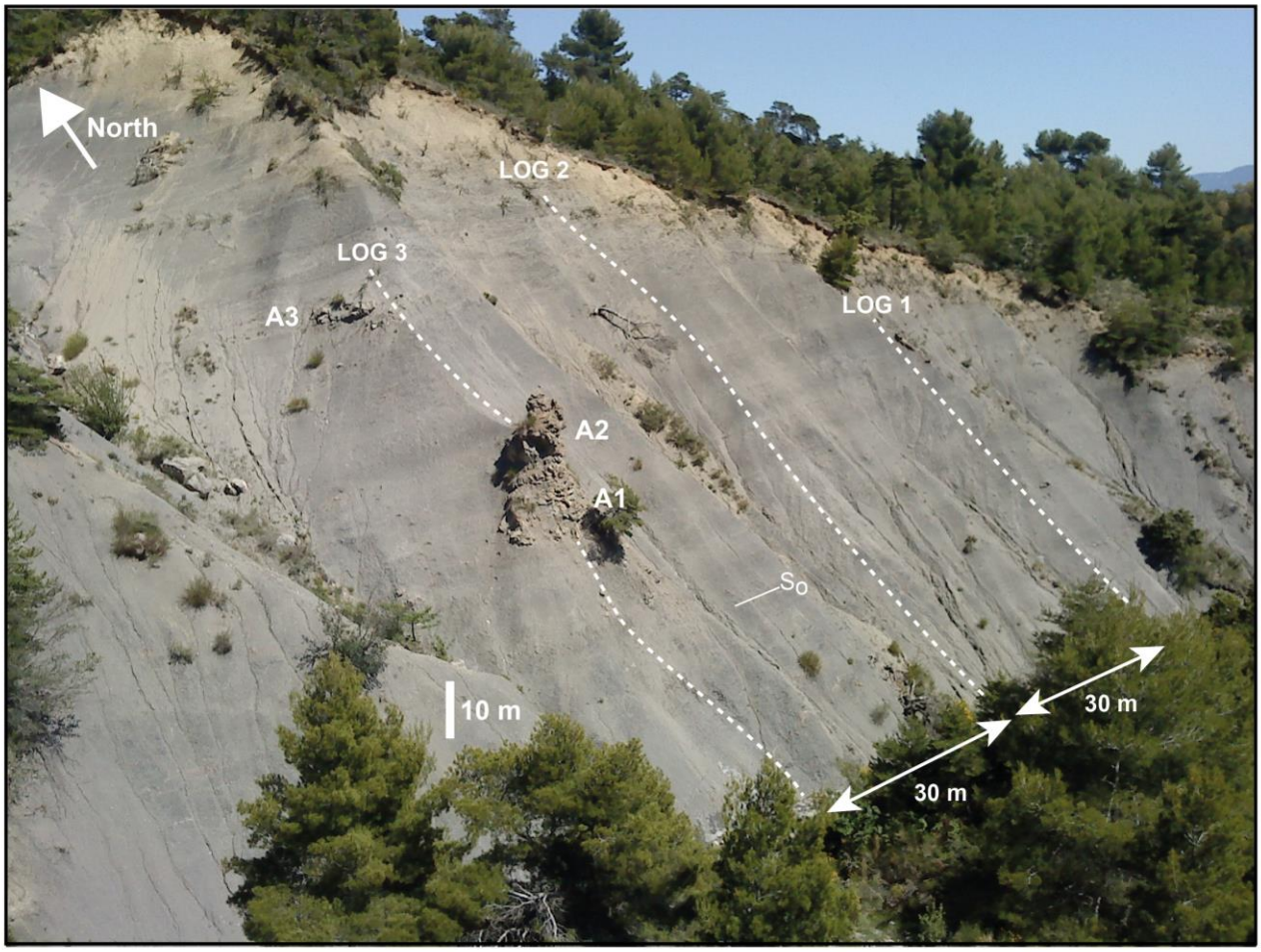

871

872 ***Figure 7: Photograph to the NE taken from site G and showing site A in the Lower Oxfordian (See Fig. 2 for location).***

873 ***Three sub-sites, A1 to A3, can be identified from to base to the top. Three high-resolution stratigraphic sections, logs***

874 ***1 to 3, were obtained at 60 m, 30 m and 0 m (vertical axis of the 3 sub-sites A1 to A3).***

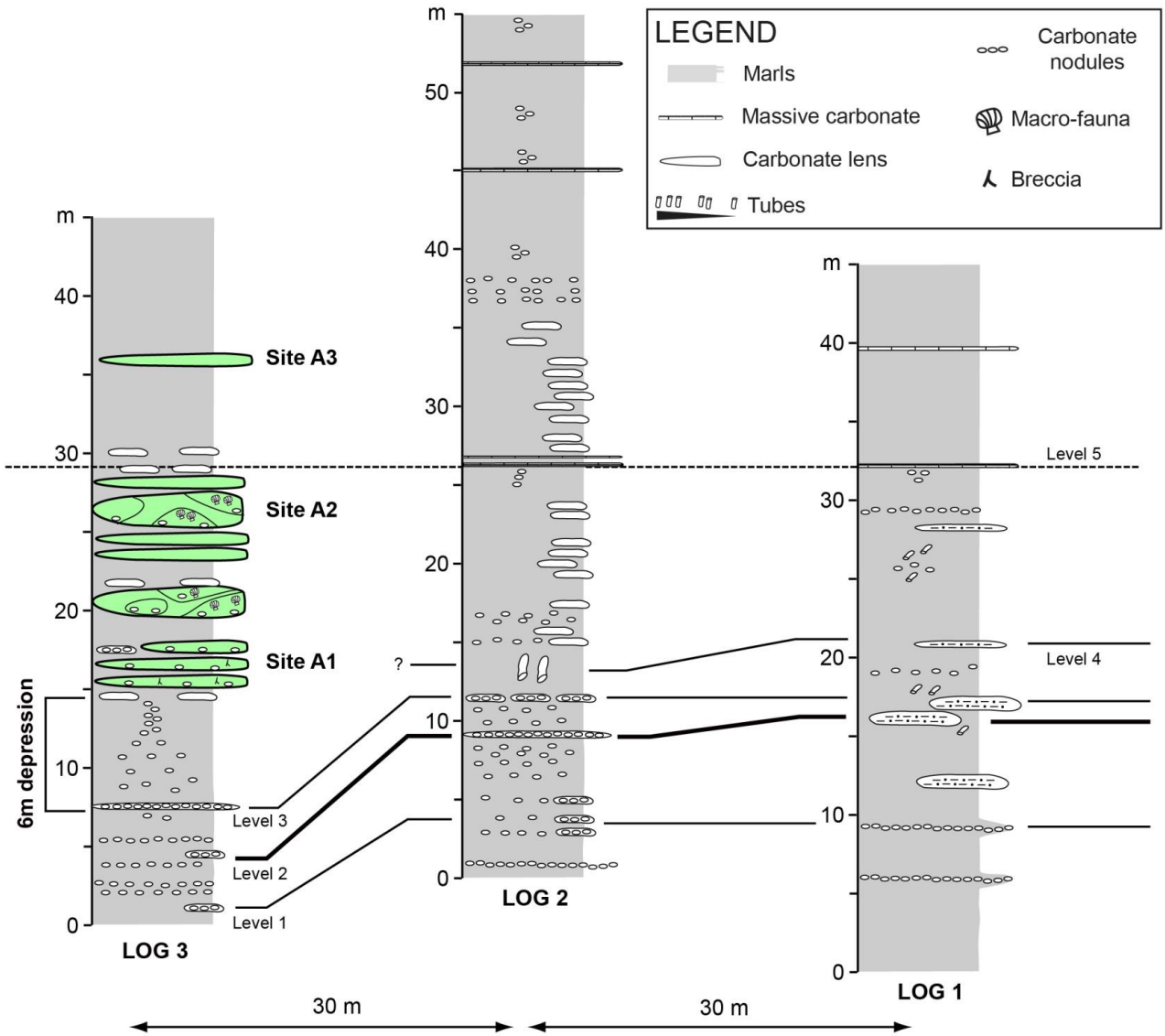

875

876 ***Figure 8: Sedimentological logs 1 to 3 obtained at site A (see Fig. 2 for location, see Fig. 7 the detailed location). All***
877 ***sections were flattened on level 5 located on top of sub-site A2 in log 3. Levels 1 to 3 are located 4 to 6 m beneath***
878 ***the general stratigraphy at the base of log 3 defining a smooth depression. All levels are marked by a decrease in***
879 ***nodule concentrations from log 3 to log 1.***

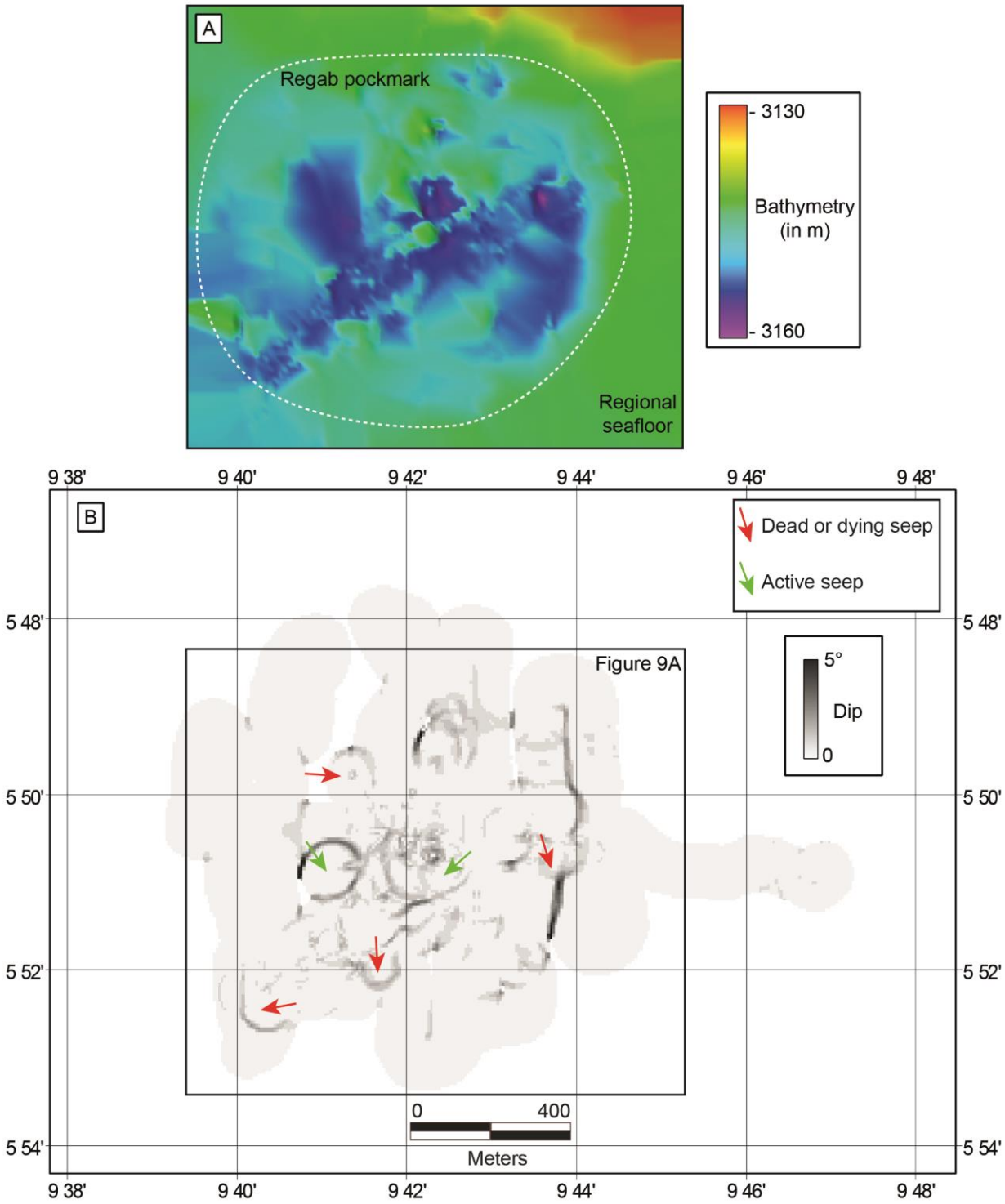

Figure 9: A) High resolution bathymetric map of the Regab pockmark, acquired during the Zairov and Biozaire scientific surveys in 2000-2002. B) Dip map of the Regab pockmark obtained by deriving the bathymetric map. It shows well expressed 100 m wide sub-circular depressions. Green arrows represent the depressions with active and high concentration methane seepage corresponding to the most active area (Gay et al. 2006). Red arrows represent intermediate or low methane flow rates interpreted as dormant or dying sub-sites.

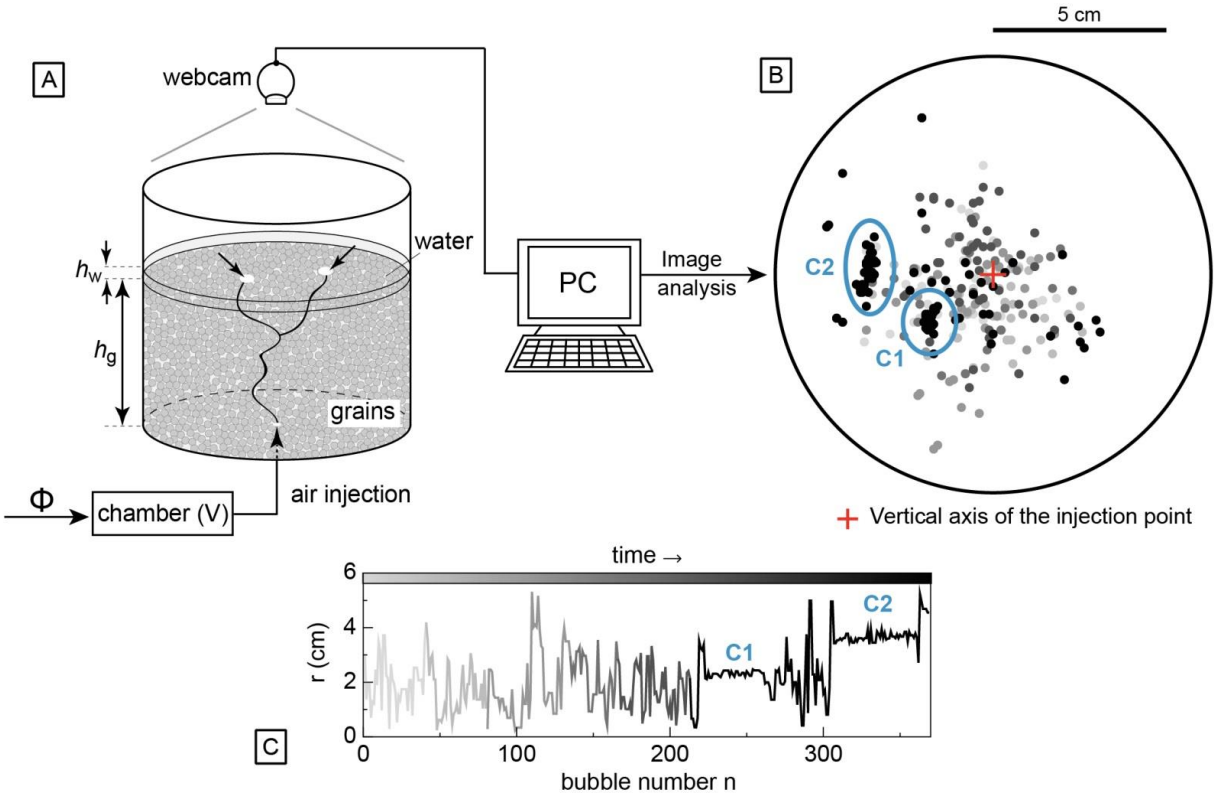

Figure 10: 3D sandbox experiment (Varas et al. 2015). A) Experimental setup. Air is injected at a constant flow rate Φ at the bottom of an immersed granular column (h_g is the height of grains and h_w the height of water above the granular bed). Bubble emission at the free surface is recorded by a webcam positioned over the experimental cell. B) Detection of bubble emission at the free surface [d = 318 ± 44 µm, hg = 14 cm, hg = 2 cm, Φ = 4.3 mL/s; the dots color from light gray to black is proportional to time]. The system releases bubbles in different (uncorrelated) positions. For two significant periods of time, however, several successive bubbles are emitted in a narrow region (clusters C1 and C2). It indicates the formation of a gas channel fixed at depth (region C1), which then collapses before it can reopen in another region (C2). C) Distance r between the bubble emission location and the centre of the cell (red cross in B) as a function of the bubble number n for the sequence presented in B.

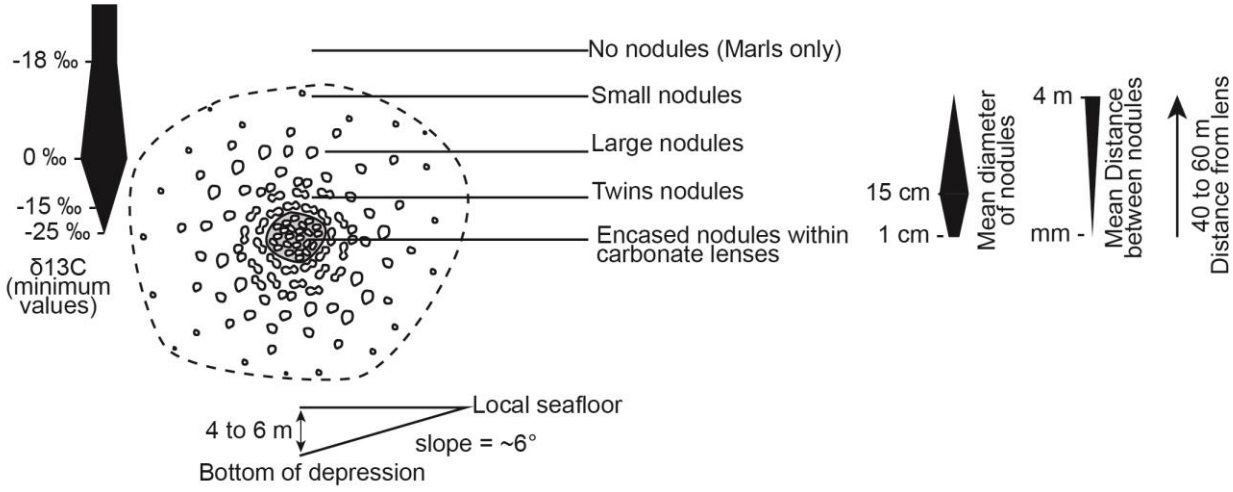

Figure 11: Schematic diagram of the organization of a single carbonate lens located in the centre of an 80 to 120 m wide concentric area of nodules. Marker horizons on high resolution logs allowed the identification of a 4 to 6 m deep depression with an average slope of about 6°, which is visually almost undetectable on field.

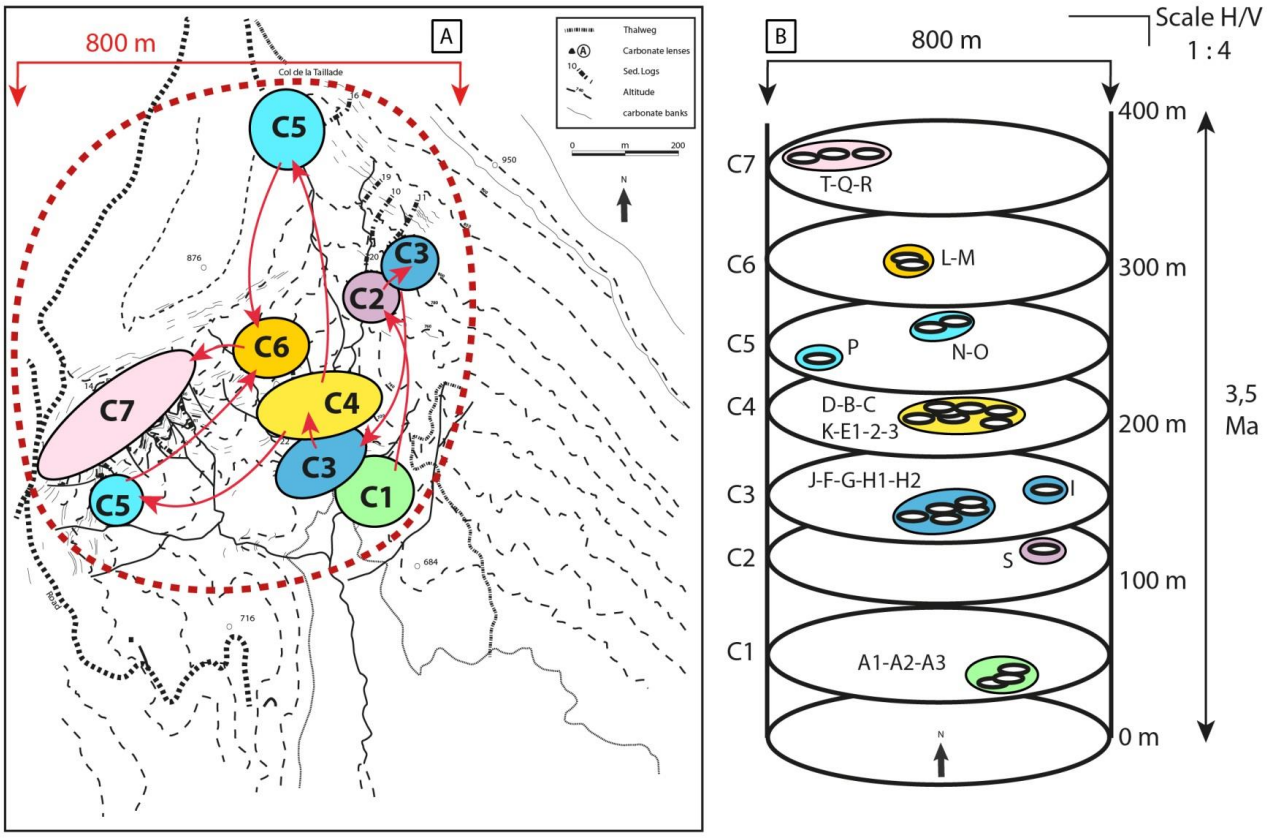

Figure 12: A) Map of the sub-sites A to T grouped by clusters regarding their stratigraphical and geographical positions in the Beauvoisin area. B) 3D schematic view of the 7 clusters showing that the point of emission at the seafloor has laterally migrated through time. The 7 periods of active seafloor fluid seepage alternated with periods of fluid quiescence for about 3.4 My, corresponding to periods of 200 ky each on average. It means that all sub-sites A to T are genetically linked and they can be grouped in an 800 m wide giant pockmark.

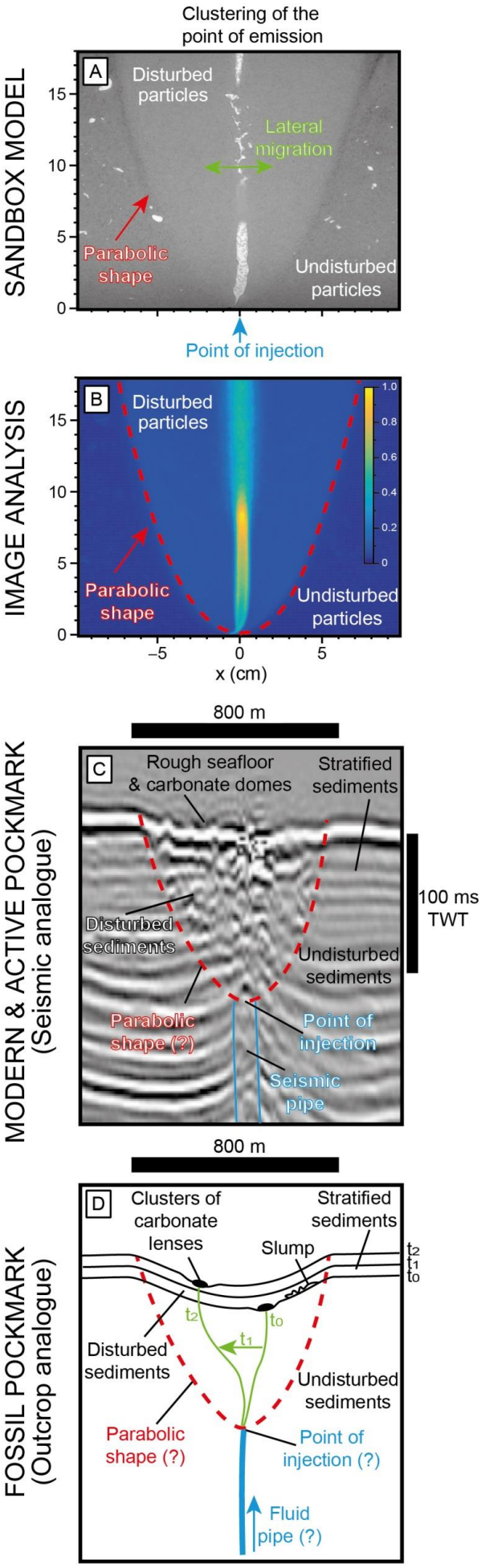
Clustering of the point of emission
SANDBOX MODEL
A
Disturbed particles
Lateral migration
Parabolic shape
Undisturbed particles
Point of injection
IMAGE ANALYSIS
B
Disturbed particles
Parabolic shape
Undisturbed particles
x (cm)
800 m
MODERN & ACTIVE POCKMARK (Seismic analogue)
C
Rough seafloor & carbonate domes
Stratified sediments
100 ms TWT
Disturbed sediments
Undisturbed sediments
Parabolic shape (?)
Point of injection
Seismic pipe
800 m
FOSSIL POCKMARK (Outcrop analogue)
D
Clusters of carbonate lenses
Stratified sediments
Slump
Disturbed sediments
Undisturbed sediments
Parabolic shape (?)
Point of injection (?)
Fluid pipe (?)

Figure 13: A) 2D sandbox experiment of air injection in a Hele-Shaw cell filled with water-saturated grains [d = 318 ± 44 µm, hg = 20 cm, h_w = 2 cm, Φ = 0.66 mL/s]. The zone where the sediments are disturbed has a roughly parabolic shape (in red), and the central gas channel displays erratic lateral motion in time (in green), leading to lateral variations of bubbles emission at the surface. B) Normalized flow density (indicated by the colorbar) computed for the series of images from which A) is extracted. High values of the flow density indicate regions where motion occurred in the system. This analysis reveals the parabolic shape of the disturbed zone (in red). C) 2D seismic profile of the Regab giant pockmark showing a disturbed zone right beneath the main depression (modified after Gay et al., 2006). The limit between undisturbed reflections and the chaotic reflections is parabolic in shape (in red). The base of the parabolic area is located on top of a vertically fractured zone (in blue) that is usually interpreted as a seismic pipe, playing the role of a feeder conduit for fluids. This facies is called the "flower" structure with a vertical narrow zone considered as the stem (i.e. the seismic pipe) feeding a wide area considered as the corolla (i.e. the disturbed sediments). D) Model of the Beauvoisin seep site considered as an outcrop analogue for a giant pockmark. In the main depression, carbonate lenses are organized in clusters that have laterally migrated through time. At time t_0 the first cluster is fed by an irregular conduit (green line). During time t_1 the conduit has collapsed, laterally shifted and reopened at a different location feeding a new cluster of carbonate lenses during time t2. It means that even if a pockmark seems dead or inactive, it could be at stage t_1 corresponding to the shifting period of the feeding conduit in the disturbed zone. However, at present neither the parabolic shape of the disturbed zone (in red), nor the feeding conduits at depth (in blue) have been identified yet.